

See discussions, stats, and author profiles for this publication at: <https://www.researchgate.net/publication/8941618>

Evaluation and comparison of 3D-QSAR CoMSIA models for CDK1, CDK5, and GSK-3 inhibition by paullones

ARTICLE in JOURNAL OF MEDICINAL CHEMISTRY · FEBRUARY 2004

Impact Factor: 5.45 · DOI: 10.1021/jm0308904 · Source: PubMed

CITATIONS

78

READS

34

12 AUTHORS, INCLUDING:



Daniel Zaharevitz

National Cancer Institute (USA)

70 PUBLICATIONS 4,166 CITATIONS

SEE PROFILE



Laurent Meijer

ManRos Therapeutics

411 PUBLICATIONS 20,688 CITATIONS

SEE PROFILE



Flemming Steen Jørgensen

University of Copenhagen

86 PUBLICATIONS 1,576 CITATIONS

SEE PROFILE

Articles

Evaluation and Comparison of 3D-QSAR CoMSIA Models for CDK1, CDK5, and GSK-3 Inhibition by Paullones

Conrad Kunick,[†] Kathrin Lauenroth,[†] Karen Wieking,[†] Xu Xie,[†] Christiane Schultz,[†] Rick Gussio,[‡] Daniel Zaharevitz,[‡] Maryse Leost,[§] Laurent Meijer,[§] Alexander Weber,^{||} Flemming S. Jørgensen,[⊥] and Thomas Lemcke^{*,†}

Institut für Pharmazie, Abteilung für Pharmazeutische Chemie, Universität Hamburg, Bundesstrasse 45, D-20146 Hamburg, Germany, Developmental Therapeutics Program, Division of Cancer Treatment and Diagnosis, National Cancer Institute, Rockville, Maryland 20852, Centre National de la Recherche Scientifique, Station Biologique, BP 74, F-29682 Roscoff, France, Department of Pharmaceutical Chemistry, University of Marburg, Marbacher Weg 6, D-35032 Marburg, Germany, and Department of Medicinal Chemistry, Danish University of Pharmaceutical Sciences, Universitetsparken 2, DK-2100 Copenhagen, Denmark

Received May 5, 2003

With a view to the rational design of selective GSK-3 β inhibitors, 3D-QSAR CoMSIA models were developed for the inhibition of the three serine/threonine kinases CDK1/cyclin B, CDK5/p25, and GSK-3 β by compounds from the paullone inhibitor family. The models are based on the kinase inhibition data of 52 paullone entities, which were aligned by a docking routine into the ATP-binding cleft of a CDK1/cyclin B homology model. Variation of grid spacing and column filtering were used during the optimization of the models. The predictive ability of the models was shown by a leave-one-out cross-validation and the prediction of an independent set of test compounds, which were synthesized especially for this purpose. Besides paullones with the basic indolo[3,2-*d*][1]benzazepine core, the test set comprised novel thieno[3',2':2,3]-azepino[4,5-*b*]indoles, pyrido[2',3':2,3]azepino[4,5-*b*]indoles, and a pyrido[3',2':4,5]pyrrolo[3,2-*d*][1]benzazepine. The best statistical values for the CoMSIA were obtained for the CDK1-models ($r^2 = 0.929$ and $q^2 = 0.699$), which were clearly superior to the models for CDK5 ($r^2 = 0.874$ and $q^2 = 0.652$) and GSK-3 ($r^2 = 0.871$ and $q^2 = 0.554$).

Introduction

Glycogen synthase kinase-3 (GSK-3) is a serine/threonine kinase, which is ubiquitously expressed in mammalian tissues and interferes with a number of signaling processes. Two isoforms of GSK-3 exist, designated GSK-3 α and GSK-3 β . While these isoforms share a high homology at their catalytic site, the α -form possesses an extended N-terminus with respect to the β -form. The phosphorylation of proteins by GSK-3 is an important link in signaling pathways that are regulating cell differentiation, cellular growth and proliferation, metabolic processes, apoptosis control, inflammation, and mechanisms involved in neuronal function. The biochemical and functional properties of GSK-3 have recently been reviewed.^{1,2} Interference with these signaling processes by the use of GSK-3-inhibiting agents bears the potential to interfere with manifold physiological or pathological situations, and consequently a high research priority is currently dedicated toward the development of small molecules with GSK-3-inhibitory properties.^{3,4} For instance, GSK-3 has been identified

as an important kinase in the intracellular signaling pathway downstream from the insulin receptor.⁵ GSK-3 inactivates glycogen synthase by phosphorylation, resulting in glycogen synthesis inhibition. Following the interaction of insulin with its receptor in the plasma membrane, a signaling cascade leads to activation of protein kinase B (PKB, also called Akt), which in turn deactivates GSK-3 by phosphorylation. In this situation the unphosphorylated glycogen synthase remains active, and glycogen synthesis is stimulated. Thus, the inhibition of GSK-3 by kinase inhibitors has been suggested as a potential principle for the development of antidiabetic therapeutics.^{3,6} Treatment of cultured human skeletal muscle cells with lithium, which is thought to inhibit GSK-3 by competition for magnesium,⁷ resulted in glycogen synthase activation and stimulation of glucose incorporation into glycogen.⁸ In a number of recent reports the discovery and development of structural diverse GSK-3 inhibitor classes has been described, e.g. pyridyloxadiazoles,⁹ thiadiazolidinones,¹⁰ diamino-1,2,4-triazolecarboxylic acid derivatives,¹¹ and maleimides.^{12,13} The maleimides SB-216763 and SB-415286 have been shown to stimulate glycogen synthesis in human liver cells.¹² Current advances in the search for GSK-3 inhibitors have been reviewed.⁴

Since GSK-3 is phylogenetically very closely related to the cyclin-dependent kinases (CDKs),³ it is not surprising that several kinase inhibitor classes have

* To whom correspondence should be addressed. Tel: +49-40-428383471. Fax: +49-40-428386573. E-mail: lemcke@chemie.uni-hamburg.de.

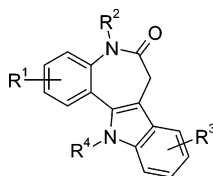
[†] Universität Hamburg.

[‡] National Cancer Institute.

[§] Centre National de la Recherche Scientifique.

^{||} University of Marburg.

[⊥] Danish University of Pharmaceutical Sciences.

Table 1. Structures and CDK1, CDK5, and GSK-3 pIC₅₀ Values for the Training Set

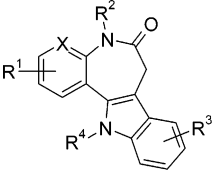
compd	NSC # ^a	R ¹	R ²	R ³	R ⁴	CDK1	CDK5	GSK-3
1	705701	H	H	9-nitro	H	7.456	7.398	8.398
2	641167	2-bromo	H	H	H	5.481	5.301	6.699
3	664704	H	H	9-bromo	H	6.398	6.071	7.638
4	672232	H	H	9-chloro	H	6.222	6.097	7.620
5	672233	H	H	11-chloro	H	5.854	5.538	6.699
6	672234	H	H	10-bromo	H	5.886	5.569	6.854
7	673433	H	H	11-bromo	H	5.886	5.770	6.222
8	675994	H	H	9-methoxy	H	6.046	5.678	5.658
9	675995	H	H	9-methyl	H	5.699	5.201	6.886
10	675996	H	H	9-fluoro	H	5.796	5.886	7.097
11	699471	4-hydroxy	H	9-bromo	H	4.398	3.071	5.367
12	699472	2,3-dihydroxy	H	9-bromo	H	5.523	5.097	6.921
13	703055	H	H	9-bromo	methyloxycarbonyl-methyl	5.854	3.456	7.125
14	700692	2-bromo	H	9-bromo	H	6.523	5.000	6.097
15	700693	2,3-dimethoxy	H	9-bromo	H	6.699	6.301	7.000
16	701589	H	methyloxycarbonyl-methyl	9-bromo	H	5.194	5.276	6.301
17	701590	H	H	9-trifluoromethyl	H	6.398	6.222	7.523
18	701591	4-methoxy	H	H	H	3.367	3.000	3.854
19	701592	2,3-dimethoxy	H	H	H	5.367	5.268	6.046
20	702373	4-methoxy	H	9-bromo	H	3.602	3.398	4.796
21	702374	H	<i>tert</i> -butyloxycarbonyl	9-bromo	<i>tert</i> -butyloxycarbonyl	3.000	N.A. ^b	3.194
22	702376	H	methyl	9-bromo	H	4.699	3.886	5.678
23	702377	H	benzyl	9-bromo	H	4.456	3.569	5.000
24	702378	2,3-dimethoxy	H	9-trifluoromethyl	H	6.553	6.367	7.125
25	703054	2-bromo	H	9-trifluoromethyl	H	6.620	5.523	5.699
26	703056	H	H	8,10-dichloro	H	5.602	3.456	5.301
27	703057	H	H	9-bromo	<i>tert</i> -butyloxycarbonyl	4.155	3.097	5.638
28	703059	H	H	9-bromo	2-hydroxyethyl	5.523	3.854	6.523
29	704071	H	H	9-bromo	methyl	5.208	3.398	6.398
30	704072	H	H	9-bromo	2-propenyl	4.222	3.620	5.398
31	704073	H	H	9-bromo	ethyl	4.638	3.585	5.824
32	704626	H	H	9-cyano	H	7.620	7.357	8.000
33	641166	H	H	H	H	5.155	4.996	6.208
34	706120	H	H	11-methyl	H	5.523	5.046	6.301
35	706121	H	ethyl	9-bromo	H	3.328	3.097	4.620
36	706122	H	H	11-ethyl	H	5.420	4.638	6.155
37	707621	2-[2-(methyloxy-carbonyl)ethenyl]	H	9-trifluoromethyl	H	5.367	4.824	6.456
38	707623	2-iodo	H	9-trifluoromethyl	H	6.155	5.155	5.658
39	707624	2-iodo	H	H	H	5.432	5.131	6.602
40	708244	2,3-dimethoxy	H	9-cyano	H	7.357	7.222	7.745
41	708245	2-[2-(1-hydroxy-cyclohexyl)ethynyl]	H	9-trifluoromethyl	H	5.495	5.081	5.699
42	708246	2-(2-cyanoethenyl)	H	9-trifluoromethyl	H	6.569	5.022	6.398
43	708247	2-(3-hydroxy-1-propynyl)	H	9-trifluoromethyl	H	6.523	5.699	6.699
44	709123	2-(2-cyanoethyl)	H	9-trifluoromethyl	H	7.328	7.481	7.481
45	709125	2,3-dimethoxy	H	9-nitro	H	7.620	7.678	7.886
46	709126	2-(3-oxo-1-butenyl)	H	9-trifluoromethyl	H	6.495	4.469	5.854
47	709129	2-bromo	H	9-nitro	H	7.276	6.921	6.699
48	684453		see Figure 1			4.481	3.155	3.456
49	702375		see Figure 1			5.638	5.097	5.699
50	704074		see Figure 1			4.367	3.347	5.921
51	708241		see Figure 1			4.292	3.066	3.745
52	708242		see Figure 1			3.886	N.A. ^b	N.A. ^b

^a Designators from the NCI antitumor drug screen. ^b Defined value not available.

been characterized to act on both GSK-3 and distinct CDKs, namely hymenialdisine,¹⁴ the indirubines,^{15–18} the aloisines,¹⁹ and the paullones.²⁰

The paullones are a family of 7,12-dihydroindolo[3,2-*d*][1]benzazepin-6(5*H*)-ones, which originally have been developed as antiproliferative CDK inhibitors.^{21–24} Among the paullones, alsterpaullone (**1**) is the most potent derivative toward GSK-3 (IC₅₀ GSK-3β = 4 nM). Although the selectivity toward only one target appears

to be a desirable feature for a potential drug, the concomitant inhibition of especially CDK5 and GSK-3 is of high interest, because both kinases are involved in the hyperphosphorylation of the tau protein. Hyperphosphorylated tau protein is the main constituent of neurofibrillary tangles, which are found as intracellular aggregates in brain cells of patients suffering from Alzheimer's disease (AD).²⁵ In AD, activation of CDK5 by the p25 protein, which is a pathological truncated

Table 2. Structures and CDK1, CDK5, and GSK-3 pIC₅₀ Values for the Test Set


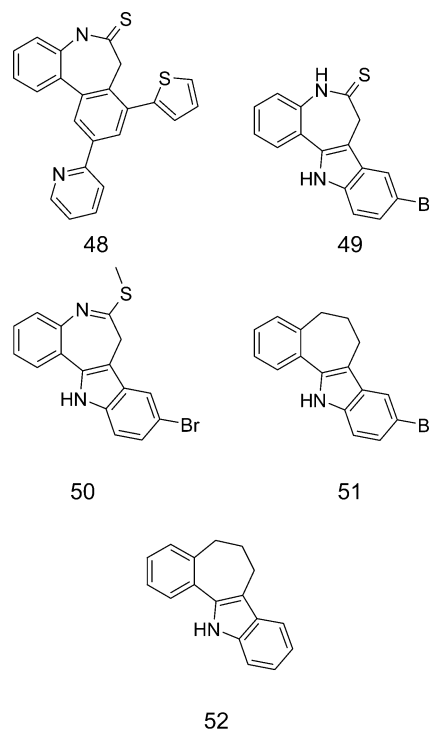
compd	NSC # ^a	X	R ¹	R ²	R ³	R ⁴	CDK1	CDK5	GSK-3
53	707622	CH	2-iodo	H	9-bromo	H	6.495	4.523	5.377
54	708243	CH	2-cyano	H	H	H	5.481	3.347	5.886
55	715966	CH	3-methoxy	H	9-trifluoromethyl	H	6.155	5.658	6.620
56	715968	CH	H	H	9-amino	H	4.699	4.523	4.921
57	716450	CH	3-hydroxy	H	9-bromo	H	6.222	6.081	7.745
58	716451	CH	H	H	9-acetylamino	H	5.886	5.260	4.387
59	716453	N	H	H	9-methoxy	H	4.046	3.377	N.A. ^b
60	718539	CH	2-(2-oxopropyl)	H	9-trifluoromethyl	H	6.699	6.377	7.046
61	718541	N	H	H	9-chloro	H	4.638	4.377	3.301
62	719342	N	H	H	9-trifluoromethyl	H	5.222	4.886	5.276
63	719343	CH	3-methoxy	H	9-cyano	H	5.921	6.000	6.886
64	720309	CH	3-methoxy	H	9-nitro	H	6.000	6.201	7.155
65	720310	CH	2-methoxy	H	9-nitro	H	7.097	7.155	7.658
66	720311	N	H	H	9-methyl	H	3.699	3.367	N.A. ^b
67	709128			see Figure 2			5.658	5.481	5.260
68	716452			see Figure 2			5.886	5.770	6.222
69	716784			see Figure 2			3.638	3.071	3.000
70	716977			see Figure 2			6.155	3.377	7.523

^a Designators from the NCI antitumor drug screen. ^b Defined value not available.

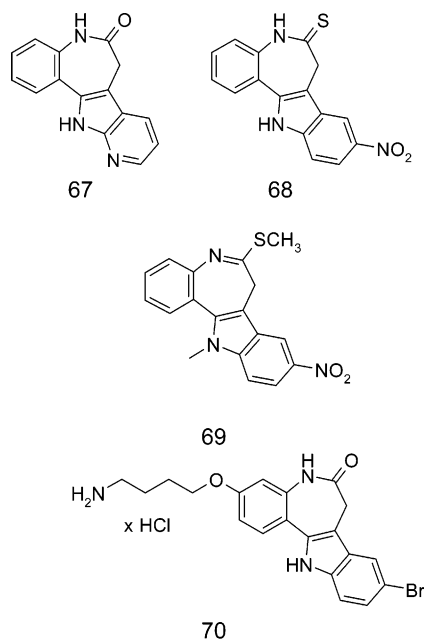
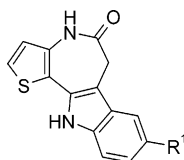
version of the physiological CDK5 activator p35, leads to tau hyperphosphorylation.^{26,27} On the basis of these and other observations, both GSK-3^{3,4} and CDK5 inhibition^{28,29} have been suggested as putative therapeutic strategies to treat or prevent AD. It has been shown that hymenialdisine,¹⁴ indirubin-3'-monoxime,¹⁶ and alsterpaullone²⁰ inhibit the phosphorylation of human tau expressed in insect cells at phosphorylation sites specific for Alzheimer tau.

Of the above-mentioned GSK-3/CDK-inhibitors, the paullones have been most extensively explored by structural modification. For a further development in this compound family, it is not only of interest to generate compounds with enhanced kinase inhibitory property, but also to design compounds with independent CDK or GSK-3 inhibitory activity. Such compounds, which are not yet available, would be suitable for evaluating the contribution of either CDK5 or GSK-3 inhibition toward tau-phosphorylation within this family of structures. Moreover, it might make sense to suppress within this class of compounds the inhibitory activity on all other CDKs that are not involved in tau phosphorylation, such as CDK1, and CDK2, to avoid potential undesired side effects.

Here we report on the generation of a set of 3D-QSAR models, which make it possible to guide a rational design of further paullones with respect to GSK-3/CDK1/CDK5 selectivity. The models were created by comparative molecular similarity indices analysis (CoMSIA)^{30–32} using data of 52 paullones and structurally related compounds for the inhibition of GSK-3 β , CDK1/cyclin B, and CDK5/p25, respectively, which we have published previously²⁰ (Table 1). Recently reported 3D-QSAR models for the interaction of CDK1 with inhibitors from the roscovitine/purvalanol-family demonstrated the feasibility of this approach toward the molecular design of kinase inhibitors.^{33,34} In the quoted study, the 3D-QSAR models are evaluated using a test set of 79 compounds which were published independently. For

**Figure 1.** Selected compounds from the training set.

the evaluation of the models reported here, we used a test set of 23 structural diverse paullone-related compounds, which covered a broad range of kinase inhibitory activity (Tables 2 and 3). Of this set, 21 entities were especially synthesized for this purpose, including some related heterocyclic systems, namely five thieno-[3',2':2,3]azepino[4,5-*b*]indoles (**71**, **72**, **73**, **74**, **75**), four pyrido[2',3':2,3]azepino[4,5-*b*]indoles (**59**, **61**, **62**, **66**), and a pyrido[3',2':4,5]pyrrolo[3,2-*d*][1]benzazepine (**67**). Two additional paullones (**57**, **70**) from a recent paper³⁵ were also included into the test set.

**Figure 2.** Selected compounds from the test set.**Table 3.** Thieno Analogues of Paullones Included in the Test Set

compd	NSC # ^a	R ¹	CDK1 ^b	CDK5 ^b	GSK-3 ^b
71	703058	bromo	6.222	5.398	6.921
72	709124	methyl	5.398	4.398	5.886
73	709127	chloro	6.301	5.301	6.398
74	719341	cyano	7.125	6.495	6.481
75	720601	nitro	7.097	7.000	7.456

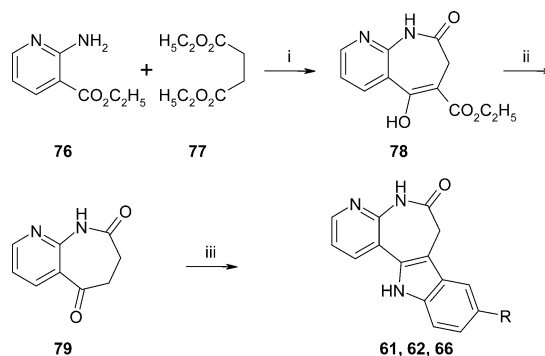
^a Designators from the NCI antitumor drug screen. ^b pIC₅₀ values.

Chemistry

The synthesis of all members of the training set has been published previously.^{20,22,36} Furthermore, preparation procedures for compounds **57** and **70** from the test set have recently been reported.^{35,37} Of the hitherto unknown members of the test set, compounds **53**, **55**, **71**, **72**, and **73** were synthesized by conventional Fischer indolization procedures, starting with known seven-membered cyclic ketones and appropriate phenylhydrazine derivatives, which were reacted in a mixture of glacial acetic acid and sulfuric acid following an established procedure without isolation of the phenylhydrazone intermediate.³⁶ However, namely in cases in which electron deficient phenylhydrazine derivatives were employed, the acid-catalyzed Fischer indolization led to unsatisfactory results. Hence, for the synthesis of the paullone derivatives **64**, **65**, **68**, and **75**, the corresponding phenylhydrazones were prepared first, and subsequently heated in refluxing diphenyl ether to yield the target compounds by means of a thermal Fischer indolization under neutral conditions.³⁸

The preparation of the cyclic ketone **79**, which was employed as a building block for the construction of 4-azapaullones, was based on commercially available 2-aminonicotinic acid ethyl ester **76**. Following a pro-

Scheme 1^a



^a (i) NaH, toluene, N₂, 90 °C, 39%; (ii) DMSO, H₂O, 150 °C, 2 h, 81%; (iii) 1. 4-R-C₆H₄-NHNH₂, HOAc, 70 °C; 2. HOAc, H₂SO₄, 70 °C, 39–64%.

tolol developed by McPhillamy et al.³⁹ for the synthesis of benzo analogues, **76** was reacted with diethyl succinate **77** in toluene in the presence of sodium hydride. The resulting cyclic enolized β -oxoester **78** was then dealkoxycarbonylated by heating in wet DMSO. The subsequent indole annelation was accomplished by applying **79** to the sulfuric acid-catalyzed Fischer reaction to yield the 4-azapaullones **61**, **62**, and **66**. When 4-methoxyphenylhydrazine was reacted with **79** in glacial acetic acid, the methoxy-substituted 4-azapaullone **59** was formed immediately without previous addition of sulfuric acid and, due to its high reactivity in the Fischer indolization reaction, the phenylhydrazone precursor of **59** was not detectable in this case (Scheme 1).

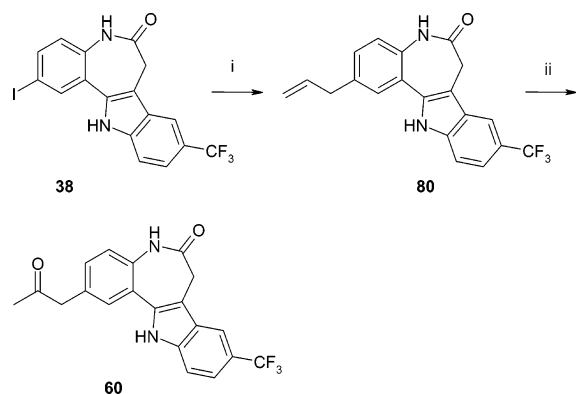
Cyano-substituted paullone congeners were prepared by means of a Rosenmund–von Braun reaction.^{40,41} Upon heating appropriate bromo compounds as starting materials with cuprous cyanide in *N*-methylpyrrolidone, the desired nitriles **54**, **63**, and **74** were obtained, albeit in poor to modest yields.

The 2-(2-oxopropyl)-9-trifluoromethylpaullone **60** was prepared in a sequence starting from the previously described iodo derivative **38**,²³ which was reacted under the conditions of a palladium-catalyzed Stille coupling with allyltributyltin to yield the 2-allyl-9-trifluoromethylpaullone **80**. The allyl moiety of **80** was subsequently air-oxidized by means of a Wacker reaction in the presence of palladium chloride and copper chloride, furnishing the oxo compound **60** in satisfactory yield (Scheme 2).

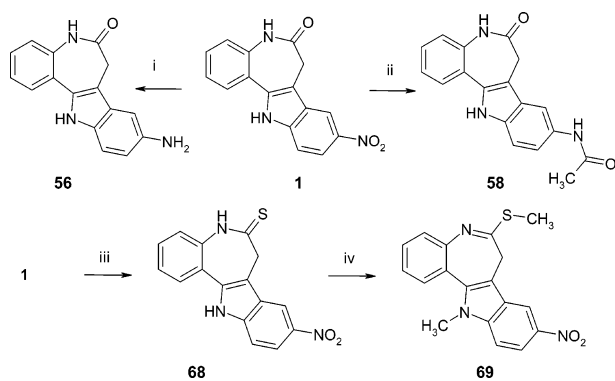
The preparation of new alsterpaullone derivatives is outlined in Scheme 3. While the reduction of alsterpaullone (**1**) with zinc powder in ethanol in the presence of calcium chloride led to 9-aminopaullone **56**, the usage of iron powder in refluxing glacial acetic acid led to the acetylated analogue **58**. Treatment of alsterpaullone (**1**) with phosphorus pentasulfide in THF gave thioalsterpaullone **68** which was dimethylated by iodomethane at both the sulfur and the indole nitrogen after deprotonation with sodium hydride to yield the thioimide **69**.

Methods and Material

Dataset. The training set for the CoMSIA calculations consisted of compounds that were published by Leost et al. in 2000.²⁰ From the original number of 56 compounds, four were discarded, because they were

Scheme 2^a

^a (i) Allyltributyltin, 10 mol % $\text{PdCl}_2(\text{PPh}_3)_2$, 20 mol % PPh_3 , DMF, 95 °C, 2 h, N_2 , 70%; (ii) 10 mol % PdCl_2 , CuCl_2 , DMF, H_2O , rt, air, 16 h, 69%.

Scheme 3^a

^a (i) Zn, EtOH, CaCl_2 , H_2O , reflux, 35% (ii) Fe, HOAc, reflux, 37%; (iii) P_2S_5 , NaHCO_3 , THF, N_2 , reflux, 3 h, 44%; (iv) NaH, H_3Cl , THF, N_2 , reflux, 4 h, 47%.

either not active (IC_{50} above 1000 μM) or had undefined stereochemistry. We ended up with a list of 52 compounds (Table 1). The test set comprised 21 newly synthesized compounds described in the chemistry section and two recently published compounds (Tables 2 and 3).³⁵ The IC_{50} values for CDK1, CDK5, and GSK-3 were converted to pIC_{50} ($-\log \text{IC}_{50}$) values and used as dependent variables in the CoMSIA calculations. The pIC_{50} values of the compounds from the training set and the test set covered an interval of more than 5 log units for all three target enzymes.

Molecular Modeling and Docking. The three-dimensional structures of all compounds in the training set and in the test set were constructed using the SYBYL program package, version 6.7 and 6.8.⁴² Because only one of the two mirror image conformations of the kenpaullone parent ring system was suitable for docking into the ATP binding site of a CDK1/cyclin B homology-model,²⁴ the corresponding azepine ring conformer was used as a template to model all paullone derivatives used in this study. Partial atomic charges were calculated using the semiempirical program MOPAC 6.0, applying the AM1 Hamiltonian.⁴³ Energy minimizations were performed using the Tripos force field⁴⁴ with a distance dependent dielectric and the Powell conjugate gradient algorithm with a convergence criterion of 0.005 kcal/(mol Å) and max. 10000 iterations, respectively, and taking charges into account.

All compounds of the training set and the test set were manually docked into the ATP binding pocket of the above-mentioned CDK1/cyclin B model from Gussio et al.,²⁴ using the already docked kenpaullone scaffold as a template. All inhibitor–protein complexes were minimized using the MAB force field^{45,46} as implemented in the program MOLOC, keeping the protein fixed and allowing the inhibitor to move.

CoMSIA. For the alignment in the CoMSIA analysis, the relative three-dimensional orientations of the compounds included in the training set and the test set resulting from the MOLOC minimizations were used (Figure 3a,b). This resulted in an alignment that most likely represents the bioactive conformation of the paullones in the CDK1 binding site. Partial atomic charges were recalculated as indicated above, using the AM1 as implemented in MOPAC. A 3D cubic lattice box with a grid spacing of 2 Å or 1 Å was created around the aligned molecules. The five CoMSIA similarity index fields available within SYBYL (steric, electrostatic, hydrophobic, hydrogen bond donor and acceptor)^{30–32} were calculated using a C^{1+} probe of a 1 Å radius and the default value of 0.3 as attenuation factor.

The CoMSIA fields were used as independent variables, and the pIC_{50} values as dependent variables in a partial least squares (PLS)⁴⁷ regression analysis, to derive 3D-QSAR models. To determine the optimal number of components the SAMPLS algorithm⁴⁸ (as implemented within SYBYL) was used. The number of components corresponding to the lowest *PRESS* (predictive sum of squares) value was used for deriving the subsequent PLS models. Cross-validation was performed using the leave-one-out method (LOO) with a column filtering of 0.5, 1.0, and 2.0 to calculate q^2 (predictive r^2) and *PRESS* to check the predictiveness of the corresponding model. Finally nonvalidated models were produced and the corresponding conventional correlation coefficient r^2 , its standard error *s*, and the *F*-ratio were computed (Tables 4 and 5). The stdev*coeff contour maps for all five CoMSIA fields were produced and analyzed for each enzyme.

For a compression of the amino acids forming the ATP binding pocket of CDK1, CDK5, and GSK-3, respectively, a multiple sequence alignment was done with the program ClustalW⁴⁹ at the ClustalW WWW Service at the European Bioinformatics Institute (<http://www.ebi.ac.uk/clustalw>), using the sequences of CDK1 (Q17066),⁵⁰ CDK5 (Q00535),⁵¹ and GSK-3 (P49841),⁵² that were retrieved from the SwissProt database⁵³ and a default setup (default matrix type: Gonnet 250).

Results and Discussion

Alignment. In 3D-QSAR studies the spatial alignment of the compounds is usually one of the key steps in order to obtain meaningful results. The biologically active conformations of the structures should be aligned in a way representing a similar binding mode. In the case that the biologically active conformation is not known, the lowest energy conformation of each structure is usually aligned on the basis of a common structural feature.

In a preliminary study with our dataset,⁵⁴ an alignment of the compounds on the basis of the seven-membered lactam ring system of the energy-minimized

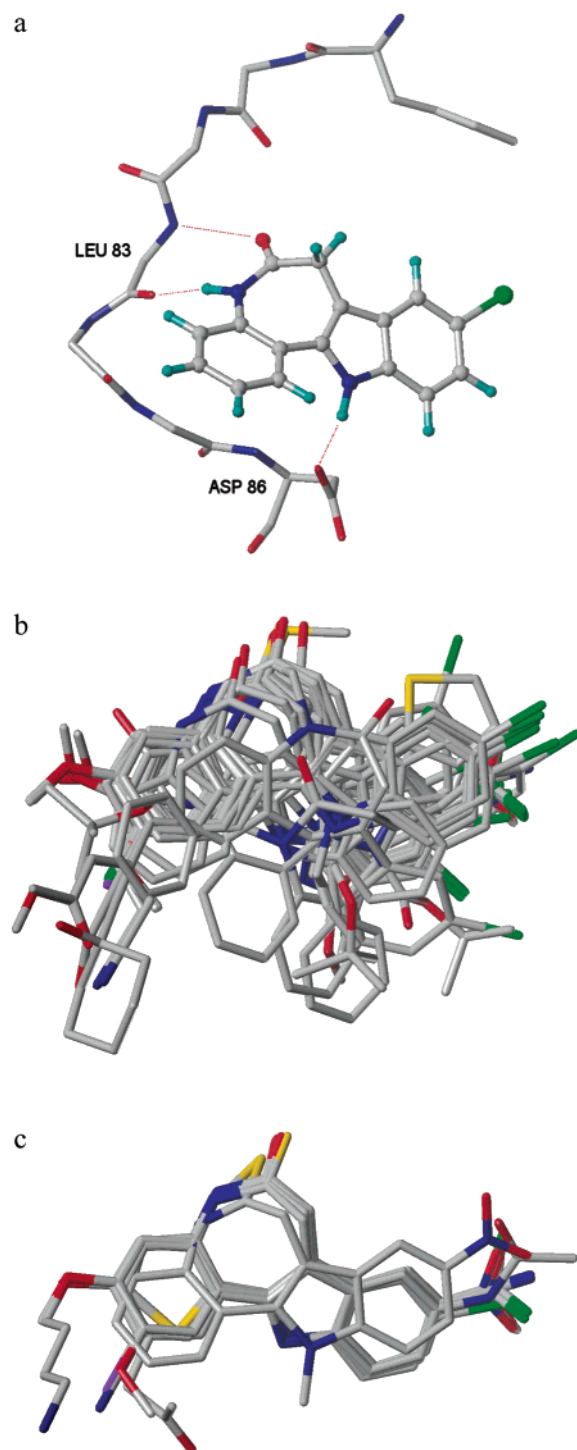


Figure 3. (a) Spatial orientation of kenpaullone **3** in the binding site. Hydrogen bonds with Leu83 and Asp86 are depicted by dotted lines. (b) View of the alignment of all compounds of the training set. (c) View of the alignment of all compounds of the test set.

structures was carried out and produced only moderate q^2 and r^2 values. Therefore, we concluded, that the ligand side chain conformation is of critical importance to the biologically active conformations, and consequently we used a docked alignment.

Since there is no X-ray crystallographic structure information about the biologically active conformation of paullones binding to CDK1/cyclin B, we used a model of kenpaullone docked into the ATP-binding site of a

Table 4. Summary of the CoMSIA Models

	CDK1 ^a		CDK5 ^b		GSK3 ^c	
step size	2 Å	1 Å	2 Å	1 Å	2 Å	1 Å
col. filt.	0.5	0.5	0.5	0.5	0.5	0.5
no. used columns	1158	9275	1158	9275	1158	9275
q^2	0.699	0.691	0.652	0.649	0.546	0.548
PRESS	0.663	0.671	0.846	0.849	0.861	0.859
r^2	0.929	0.929	0.874	0.871	0.874	0.874
s	0.321	0.323	0.509	0.515	0.454	0.453
F	120.916	119.6	81.422	79.520	63.544	63.865
opt. no. compon.	5	5	4	4	5	5
stepsize	2 Å	1 Å	2 Å	1 Å	2 Å	1 Å
col. filt.	1.0	1.0	1.0	1.0	1.0	1.0
no. used columns	907	7139	907	7139	907	7139
q^2	0.697	0.689	0.651	0.649	0.548	0.550
PRESS	0.665	0.673	0.847	0.849	0.859	0.857
r^2	0.928	0.928	0.872	0.870	0.873	0.874
s	0.324	0.325	0.512	0.517	0.455	0.454
F	118.793	117.766	80.323	78.726	63.274	63.555
opt. no. compon.	5	5	4	4	5	5
stepsize	2 Å	1 Å	2 Å	1 Å	2 Å	1 Å
col. filt.	2.0	2.0	2.0	2.0	2.0	2.0
no. used columns	632	4971	632	4971	632	4971
q^2	0.692	0.686	0.652	0.649	0.552	0.554
PRESS	0.670	0.676	0.846	0.850	0.855	0.853
r^2	0.927	0.926	0.871	0.866	0.870	0.871
s	0.325	0.329	0.514	0.525	0.460	0.458
F	117.474	114.559	79.581	76.124	61.837	62.292
opt. no. compon.	5	5	4	4	5	5

^a The best CDK1 model (in *italics*) is called *CDK1 model* in the text. ^b The best CDK5 model (in *italics*) is called *CDK5 model* in the text. ^c The best GSK3 model (in *italics*) is called *GSK-3 model* in the text.

Table 5. Comparison of the Statistical Values and Field Distribution within the Selected CoMSIA Models of CDK1, CDK5, and GSK-3

	CDK1 model	CDK5 model	GSK-3 model
step size	2 Å	2 Å	1 Å
col. filt.	0.5	0.5	2.0
q^2	0.699	0.652	0.554
PRESS	0.663	0.846	0.853
r^2	0.929	0.874	0.871
s	0.321	0.509	0.458
F	120.916	81.422	62.292
opt. no. components	5	4	5
field contribution			
steric	0.087	0.092	0.084
electrostatic	0.253	0.236	0.178
hydrophobic	0.181	0.227	0.232
donor	0.188	0.169	0.213
acceptor	0.290	0.277	0.293

CDK1/cyclin B model²⁴ as a template for our docking. In this model the indolobenzazepinone ring system is sandwiched between the lipophilic side chains of Ile10 and Leu134. Three hydrogen bonds are observed (azepine NH–Leu83 backbone carbonyl, azepine carbonyl–Leu83 backbone NH, indole NH–Asp86 side chain carbonyl) that fix the structures in a similar spatial position.

After manually docking all structures of the training set and the test set into the CDK1 binding site, we minimized all inhibitor–protein complexes with the MAB-force field of the MOLOC program suite which uses geometric hydrogen bonding terms to model electrostatic interactions of polar groups. By this method all three hydrogen bonds of the semiempirical model from Gussio et al.²⁴ were nicely reproduced (Figure 3a). The resulting relative conformations of all compounds

in the training set and test set were used (Figure 3b,c) for the following CoMSIA calculations.

CoMSIA Models. The results of the initial CoMSIA models for a 2 Å and a 1 Å grid spacing are summarized in Table 4. For all three targets, models with a q^2 value above 0.5 could be obtained, indicating that the respective models could be useful in predicting the inhibitory activity of paullones in these targets. However, the models for CDK1 performed much better with respect to q^2 and r^2 , compared to the CDK5 or the GSK3 model. For CDK1 and CDK5 a grid spacing of 2 Å and column filtering of 0.5 resulted in the best models (CDK1: $q^2 = 0.699$, $r^2 = 0.929$, 5 components, *CDK1 model*; CDK5: $q^2 = 0.652$, $r^2 = 0.874$, 4 components, *CDK5 model*) while for GSK-3 a grid spacing of 1 Å and column filtering of 2.0 was best suited (GSK-3: $q^2 = 0.554$, $r^2 = 0.871$, 5 components, *GSK-3 model*). In an attempt to further improve our models, region focusing was used on the best initial PLS analysis, resulting in a CDK1 model with slightly better r^2 and q^2 values. However, since concomitantly the number of components necessary to derive the model rose from 5 to 7, this refinement was considered to be of minor significance and therefore the region focused CDK1 model was not pursued further. For CDK5 and GSK-3, the application of region focusing failed to improve the models. The further discussion of the CoMSIA will focus on the best models (Table 5), which will be named *CDK1 model*, *CDK5 model*, and *GSK-3 model*, respectively, as mentioned above.

An inspection of the fitted predictions for the best CoMSIA models (Table 6 and Figure 4) revealed that three compounds from the training set (**44**, **26**, and **11**) were poorly predicted in the CDK5 and GSK-3 models. In the case of **44** this could be caused by the relative flexibility of the cyanoethyl side chain. Since we used a docked alignment with the 3D structure of CDK1 as template, the side chain conformation is optimized for CDK1 only, but might be different in CDK5 or GSK-3. **11** is the only 4-hydroxypaullone and **26** the only 8,10-disubstituted paullone in the dataset. This structural uniqueness might be the reason that both structures are poorly predicted in the CDK5 and GSK-3 models. Even though the deletion of these compounds from the training set would have improved the statistical results for the CDK5 and GSK-3 models, we decided to keep them in the dataset because they still might contribute valuable information for the entire model.

The ultimate test for the usefulness of a 3D-QSAR model in the drug design process is predicting the activity of new compounds that are not included in the dataset that was used to obtain the model. The CoMSIA models reported here were challenged with a test set comprising 23 newly synthesized paullone derivatives. Among the members of this set were paullones representing structures similar to the training set compounds and some derivatives with new structural features (4-azapaullones **59**, **61**, **62**, and **66**, as well as the thiophene analogues **71**, **72**, **73**, **74**, and **75**). The predicted pIC_{50} values for the test set are summarized in Table 7 and Figure 4. On first sight the prediction of the inhibitory activities for CDK1, as was to be expected from the q^2 of the corresponding QSAR model, is better than for

Table 6. Residuals of the Training Set

compd	CDK1		CDK5		GSK-3	
	pIC_{50}	fitted prediction	pIC_{50}	fitted prediction	pIC_{50}	fitted prediction
1	7.46	7.31	7.40	7.17	8.40	7.90
2	5.48	5.76	5.30	5.09	6.70	5.98
3	6.40	6.13	6.07	5.59	7.64	7.14
4	6.22	6.11	6.10	5.55	7.62	6.98
5	5.85	5.63	5.54	5.39	6.70	6.29
6	5.89	5.73	5.57	5.17	6.85	6.41
7	5.89	5.67	5.85	5.56	6.05	6.37
8	6.05	5.87	5.68	5.61	5.66	6.64
9	5.70	5.85	5.20	5.42	6.89	6.76
10	5.80	6.05	5.89	5.65	7.10	6.89
11	4.40	5.00	3.07	4.13	5.37	6.14
12	5.52	5.26	5.10	4.79	6.92	6.75
13	5.85	5.72	3.46	2.98	7.13	7.11
14	6.52	6.18	5.00	5.17	6.10	6.55
15	6.70	6.51	6.30	6.26	7.00	7.16
16	5.19	5.03	5.28	5.28	6.30	5.68
17	6.40	6.31	6.22	5.71	7.52	6.92
18	3.37	2.78	3.00	2.42	3.85	3.35
19	5.37	6.09	5.27	6.18	6.05	6.60
20	3.60	3.60	3.40	3.25	4.80	4.68
21	3.00	3.00	3.00	3.13	3.19	3.36
22	4.70	4.34	3.89	3.30	5.68	5.21
23	4.46	4.26	3.57	4.07	5.00	4.68
24	6.55	6.71	6.37	6.53	7.13	6.90
25	6.62	6.37	5.52	5.44	5.70	6.29
26	5.60	5.67	3.46	4.82	5.30	6.11
27	4.16	4.39	3.10	2.85	5.64	5.77
28	5.52	5.59	3.85	3.57	6.52	6.82
29	5.21	5.00	3.40	3.48	6.40	6.16
30	4.22	4.61	3.62	3.65	5.40	5.79
31	4.64	4.81	3.58	3.64	5.82	6.05
32	7.62	7.16	7.36	6.65	8.00	7.89
33	5.52	5.59	5.05	5.29	6.30	6.37
34	3.33	3.98	3.10	3.51	4.62	4.93
35	5.42	5.45	4.64	5.20	6.16	6.23
36	5.16	5.69	5.00	5.37	6.21	6.60
37	5.37	5.60	3.89	4.09	6.05	5.89
38	6.16	6.39	5.16	5.37	5.66	6.18
39	5.43	5.80	5.13	5.04	6.60	5.88
40	7.36	7.55	7.22	7.46	7.74	7.87
41	5.49	5.08	5.08	4.83	5.70	5.36
42	6.57	6.80	5.02	5.86	6.40	6.80
43	6.52	6.59	5.70	5.74	6.70	6.68
44	7.33	6.87	7.48	5.98	7.48	6.84
45	7.62	7.68	7.68	7.93	7.89	7.88
46	6.49	6.03	4.47	4.28	5.85	5.78
47	7.28	7.34	6.92	6.86	6.70	7.25
48	4.48	4.11	3.15	2.93	3.46	3.23
49	5.64	5.44	5.10	4.60	5.70	5.59
50	4.37	4.48	3.35	3.50	5.92	5.80
51	4.29	4.74	3.07	3.89	3.74	4.49
52	3.89	3.93	3.00	3.39	3.00	3.29

CDK5 or GSK-3. On closer inspection some additional details are observed.

In all three models the 4-azapaullones (**59**, **61**, **62**, **66**) and the 3-methoxy-substituted paullones (**63**, **64**) were clearly overpredicted. This observation can be explained with the absence of similar compounds in the training set that could contribute required information to the model regarding the 4- or 3-position, respectively. Similarly, the thioimide **69** was overpredicted, although the training set comprised the thioimide **50**. However, **50** bears an unsubstituted indolo-nitrogen at position 12 that could be involved in hydrogen bonding, while **69** is lacking this feature through methyl substitution. Consequently, **69** has lost both hydrogen bond donor groups, a structural modification that could be responsible for a completely different alignment mode for **69**.

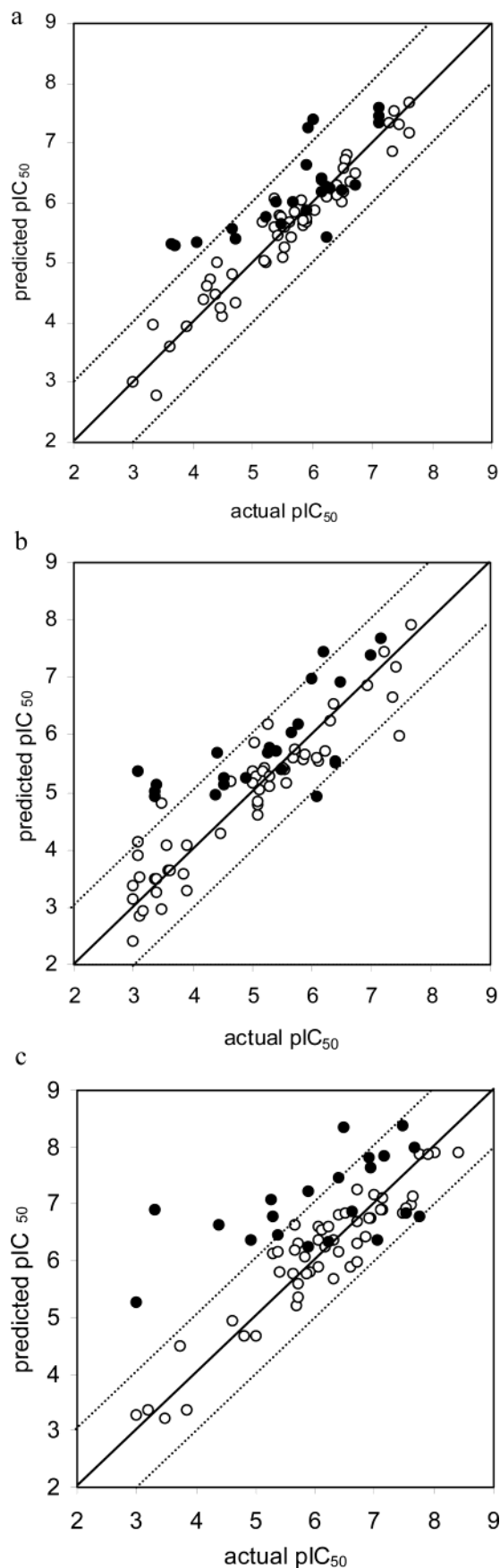


Figure 4. Plot of actual pIC_{50} vs predicted pIC_{50} for the training set (○) and the test set (●) of *CDK1* model (a), *CDK5* model (b), and *GSK-3* model (c).

The CDK1 and the CDK5 model predicted the activity of the thiophene analogues quite well, indicating that

Table 7. Predictions of the Test Set

compd	CDK1		CDK5		GSK-3	
	pIC_{50}	prediction	pIC_{50}	prediction	pIC_{50}	prediction
53	6.490	6.220	4.520	5.121	5.380	6.445
54	5.480	5.666	3.350	5.024	5.890	6.239
55	6.160	6.413	5.660	6.034	6.620	6.851
56	4.700	5.390	4.520	5.262	4.920	6.373
57	6.220	5.436	6.080	4.915	7.740	6.773
58	5.890	5.890	5.260	5.690	4.390	6.622
59	4.050	5.334	3.380	5.141	N.A. ^a	-
60	6.700	6.292	6.380	5.521	7.050	6.354
61	4.640	5.568	4.380	4.956	3.300	6.885
62	5.220	5.779	4.890	5.257	5.280	6.776
63	5.920	7.267	6.000	6.969	6.890	7.823
64	6.000	7.399	6.200	7.455	7.160	7.832
65	7.100	7.602	7.160	7.673	7.660	7.994
66	3.700	5.300	3.370	4.920	N.A. ^a	-
67	5.660	6.025	5.480	5.383	5.260	7.077
68	5.890	6.636	5.770	6.188	6.220	6.337
69	3.640	5.313	3.070	5.367	3.000	5.263
70	6.160	6.188	6.380	5.538	7.520	6.840
71	6.220	6.284	5.400	5.720	6.920	7.631
72	5.400	6.027	4.400	5.677	5.890	7.213
73	6.300	6.246	5.300	5.777	6.400	7.446
74	7.120	7.337	6.490	6.910	6.480	8.348
75	7.100	7.453	7.000	7.394	7.460	8.369

^a Defined values not available.

the absence of a comparable compound in the training set is not critical for these substances. In contrast, the GSK-3 model over predicted these compounds. The latter observation might be due to structural differences between the CDKs and the GSK-3 that are not explained with the alignment that was used for the training set and test set of this study.

With exception of the above-mentioned compounds, the inhibitory activities of the structures in the test set are predicted reasonably well. Consequently, we believe all three QSAR models can be used as tools in the rational design of further GSK-3 or CDK inhibitors of the paullone family.

Analysis of the 3D Contour Maps of the CoMSIA Fields. For each enzyme the contour maps for all five CoMSIA fields were produced and analyzed.

CDK1. Figure 5a,b shows the steric and electrostatic contour maps for the *CDK1* model with alsterpaullone (1) as an example for a good inhibitor and compound 27 as an example for a poor inhibitor. Sterically favored regions (colored green) appear around the nitro group at position 9 and near position 2 and 3 of the paullone scaffold, while disfavored areas (colored yellow) are located near the indole-nitrogen at position 12 and beyond the green (favorable) isopleth at position 2 and 3 of alsterpaullone. Negatively charged groups are favored near the oxygen atoms of the 9-nitro group, near the oxygen of the lactam-group at position 6, and at position 2 of the paullone ring system. A blue isopleth above the indole ring system is representing an area where positive charge is favored. The distribution of these electrostatic contours suggests that a negatively charged and electron-withdrawing substituent in the 9-position of the paullone scaffold is depleting the indole ring system of electrons, making the electrostatic potential more positive and thereby leading to inhibitors with enhanced biological activity. These findings are in good agreement with quantum mechanics calculations published recently.²⁴

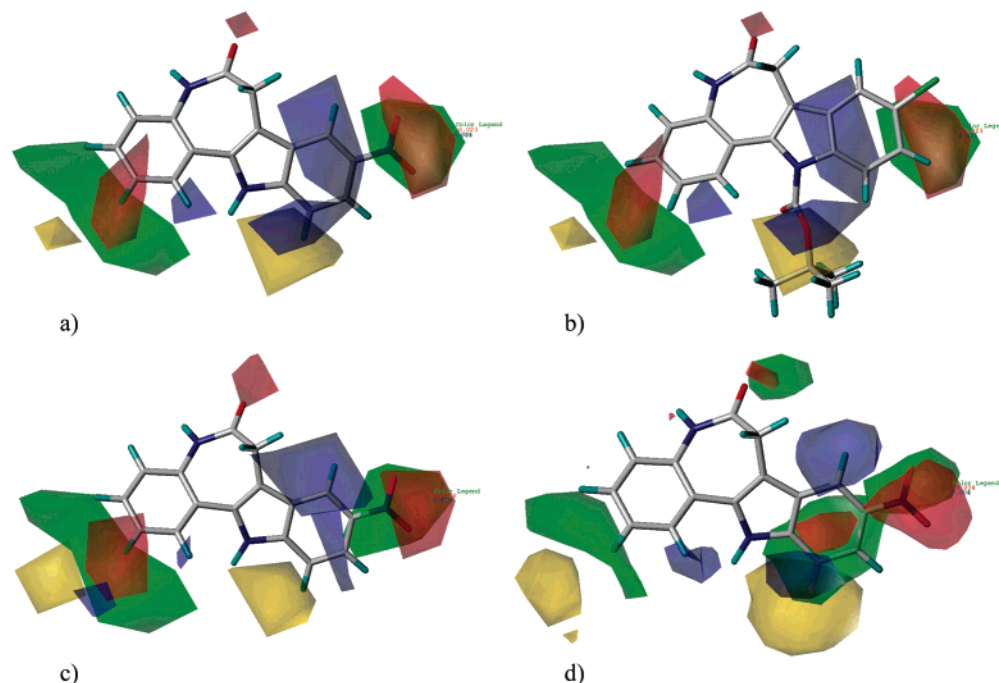


Figure 5. CoMSIA contour maps for the steric and electrostatic fields. Green contours (contour levels: CDK1: 0.006; CDK5: 0.007; GSK-3: 0.0007) indicate areas where steric bulk is favored while yellow contours (contour levels: CDK1: -0.010 ; CDK5: -0.007 ; GSK-3: -0.0015) indicate areas where it is not favored. Blue isopleths depict areas where positively charged groups increase the activity (contour levels: CDK1: 0.021; CDK5: 0.020; GSK-3: 0.004) and red isopleths indicate where negatively charged groups increase the activity (contour levels: CDK1: -0.023 ; CDK5: -0.020 ; GSK-3: -0.004). Contours of *CDK1* model (a), *CDK5* model (c), and *GSK-3* model (d) with alsterpaullone **1**. (b) Contour of *CDK1* model with compound **27**.

Substitution of the indole nitrogen, like that in compound **27**, with a boc group causes an anticlockwise shift of the whole paullone scaffold, when compound **27** is docked into the active site cavity. As a result of this shift, the bromine atom at position 9 is no longer rendered within the favored steric area. In contrast, the bromo substituent is forced away from the area where negative charge is favored. Furthermore, the butyloxy group of the 12-substituent is occupying the sterically disfavored area, and the oxygen of the ester group is placed inside the area where positive charge is favored. This is reflected by a substantial loss of inhibitory activity compared to alsterpaullone.

The contour maps of the hydrogen bond donor and acceptor fields describe the spatial arrangement of favorable and unfavorable hydrogen bond interactions to acceptor or donor groups of the target enzyme (Figure 6a,b). The cyan contours that are observed opposite the lactam hydrogen at position 5 and the indole hydrogen at position 12 describe a favorable hydrogen bond to an acceptor group in the protein, while the orange contours near the lactam oxygen at position 6 and the nitro group at position 9 indicate favorable hydrogen bonds to a hydrogen bond donor structure in the active site. Alsterpaullone fulfills these structural requirements perfectly, being able to form all four possible hydrogen bonds to the target molecule (Figure 6a). Compound **20** should in principle also be able to form these hydrogen bonds. However, the 4-methoxy group causes the ring system to rotate anticlockwise, resulting in an alignment, that places the lactam and the indole hydrogen near the purple contours which indicate unfavorable interactions between a ligand hydrogen bond donor group and the protein (Figure 6b). Consequently, compound **20** is 4 orders of magnitude less active than

alsterpaullone. A recently reported CoMSIA model for CDK1-inhibition by paullones produced contour plots with considerable different features, namely for the electrostatic field distribution.⁵⁵ These differences can easily be rationalized, taking into account that the model from the literature was constructed on the basis of a smaller number of compounds with a higher similarity, which were fitted by a rigid alignment procedure.

The contour plots of the CDK1 model nicely reflect the situation within the ATP binding site. For example, areas where steric bulk is favored are located near the entrance to the binding pocket and at the sugar pocket that would accommodate the ribose moiety of ATP (Figure 5a). The four hydrogen bonds that are assumed to render the paullones in the binding pocket are also accurately visualized by the contour plots. Thus, while the cyan contours depicted in Figure 6a represent the backbone carbonyl of Leu83 and the side chain carboxylate of Asp86, the orange contours match the backbone NH of Leu83 as well as a water molecule reported to be located near the aromatic ring of Phe80.

CDK5. For CDK5, the spatial distribution of favorable and unfavorable contours is nearly identical, while the relative size varies a little compared to CDK1 (Figures 5c and 6c). This similarity is corresponding to the high degree of conservation of the amino acid sequence within the ATP binding sites of CDK1 and CDK5. A multiple sequence alignment, done with ClustalW, revealed that only three active site residues vary between the sequence of our CDK1 model and the sequence of CDK5 (Leu83–Cys83; Thr84–Asp84; Met85–Glu85). All three residues present their backbone to the binding site cavity, while their side chains point away from the

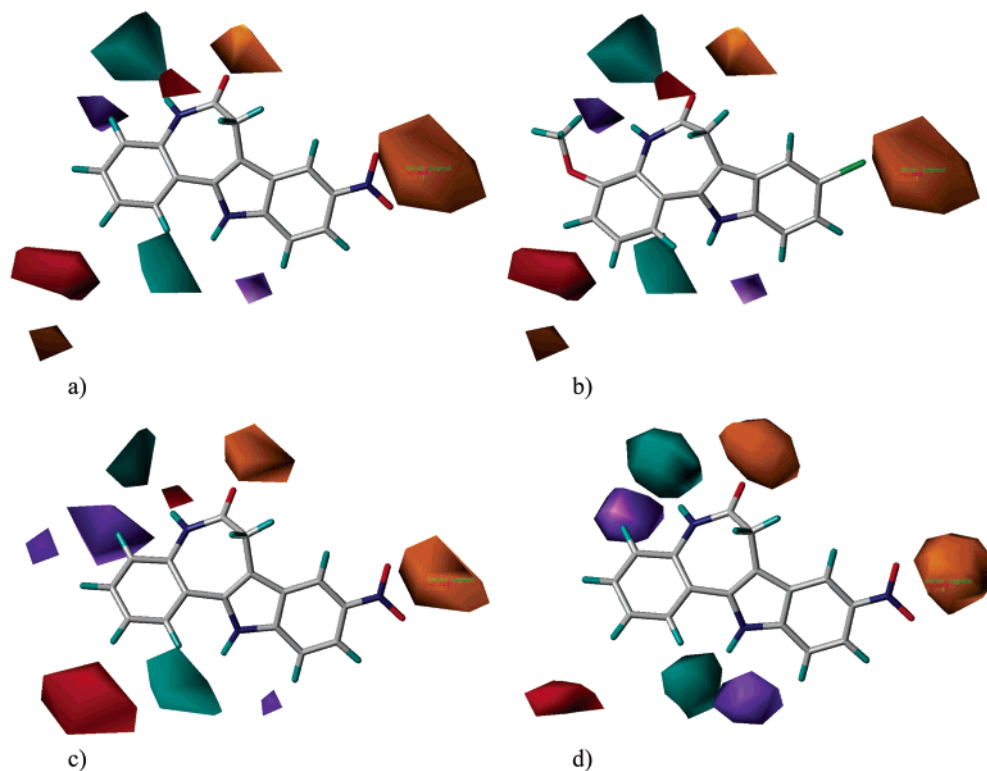


Figure 6. CoMSIA contour maps for the hydrogen bond donor and acceptor fields. Cyan contours (contour levels: CDK1: 0.035; CDK5: 0.04; GSK-3: 0.009) indicate areas where an acceptor group in the protein forms favorable hydrogen bonds to a donor group of the ligand, while orange contours (contour levels: CDK1: 0.032; CDK5: 0.04; GSK-3: 0.008) indicate areas where a donor group in the protein forms favorable hydrogen bonds to an acceptor group of the ligand. The purple contours (contour levels: CDK1: -0.0041 ; CDK5: -0.025 ; GSK-3: -0.0085) and the red contours (contour levels: CDK1: -0.016 ; CDK5: -0.021 ; GSK-3: -0.0035) indicate areas where an acceptor or a donor group, respectively, in the protein would form unfavorable hydrogen bonds to the ligand. Contours of *CDK1* model (a), *CDK5* model (c), and *GSK-3* model (d) with alsterpaullone **1**. (b) Contour of *CDK1* model with compound **20**.

cavity. Hence, the architecture of the ATP binding site of CDK1 and CDK5 can be considered as rather similar.

GSK-3. The contour maps of GSK-3 are different to the ones of CDK1 and CDK5. The steric field shows two additional favorable contours below the lactam oxygen at position 6 and around the benzo annelated of the indole substructure, respectively (Figure 5d). With respect to the electrostatic field, a much larger blue isopleth (positive charge favored) near the 1 position is observed in GSK-3, while the large red contour indicating a favorable interaction for negative charges near the position 2, as found in the CDK1 and CDK5, is missing. Moreover, in GSK-3 the blue isopleth above the indole ring system observed in CDK1 and CDK5 is divided into two areas that are located above the 8- and the 11-position of the paullone ring system. An additional area of favorable negative charge (colored red) is found slightly below the indole ring system.

Only slight differences were found when the hydrogen bonding contour maps of the GSK-3 model were compared to the CDK1 and CDK5 models, respectively (Figure 6d).

Conclusion

Three CoMSIA models have been developed, which describe the three-dimensional structure activity relationships for the kinase-inhibitory activity of paullones with respect to CDK1, CDK5, and GSK-3 β . The models are characterized with conventional r^2 of 0.929, 0.874, and 0.871, respectively, and cross-validated with q^2

coefficients of 0.699, 0.652, and 0.554, respectively. Differences in the 3D contour plots for inhibition of the three enzymes show that a rational design of paullones directed toward selective GSK-3 or CDK inhibition should be possible by the application of the three models. Namely the differences in the electronic fields between the models should be taken into account for the further development of GSK-3-selective paullones. In the course of our future research, new compounds with modified electron density throughout the heterocyclic ring system will be designed and be evaluated in the CoMSIA models *in silico* before synthetic approaches are undertaken.

Experimental Section

Synthetic Chemistry. Melting points (mp) were determined on an electric variable heater (Electrothermal 9100) and were not corrected. Elemental analyses were performed in the analytical departments of the Fachbereich Chemie, Universität Hamburg. Results obtained were within $\pm 0.4\%$ unless indicated otherwise. Nuclear magnetic resonance spectra were recorded on a Bruker AMX 400 instrument, using tetramethylsilane as internal standard and dimethyl sulfoxide- d_6 as solvent unless stated otherwise. NMR signals are reported in ppm on a δ scale. High-resolution FAB mass spectra (FAB-HMRS) were determined on a Finnigan MAT 311A instrument using 3-nitrobenzyl alcohol as matrix. EI/HRMS spectra were recorded on a VG 70-250S double focusing mass spectrometer. Column chromatography was performed using chromatography grade silica gel 60 (Merck). Thin-layer chromatography (TLC) was performed using fluorescent Polygram Sil G/UV₂₅₄ silica gel plates. Spots were visualized under 254 nm UV illumination.

General Procedure A for Preparation of Paullone Derivatives 53, 55, 61, 62, 66, 71, 72, 73, by Acid-Catalyzed Fischer Indole Reaction. To a slurry of an appropriate cyclic ketone (1 mmol) in glacial acetic acid (2 mL) is added dropwise a suspension of the appropriate corresponding phenylhydrazine (1.5 mmol) [or the appropriate substituted phenylhydrazine hydrochloride (1.5 mmol) and sodium acetate (123 mg, 1.5 mmol)] in glacial acetic acid (5 mL) with stirring. After being stirred at 70 °C for 1 h, the mixture is cooled to room temperature. Concentrated sulfuric acid (0.1 mL) is added, and stirring is continued at 70 °C. The reaction is monitored by TLC (eluent: ethyl acetate or toluene/acetone 1:1, respectively). Portions of concentrated sulfuric acid (0.1 mL) are added each 1.5 h until completion of the reaction is detected. After being cooled to room temperature, the mixture is poured into a 5% aqueous sodium acetate solution (15 mL). A precipitate is formed, which is filtered off with suction and purified by crystallization from the given solvent.

9-Bromo-2-iodo-7,12-dihydro-indolo[3,2-*d*][1]benzazepin-6(5*H*)-one (53). Preparation following General Procedure A from 7-iodo-1*H*-[1]benzazepine-2,5(3*H*,4*H*)-dione²³ and 4-bromophenylhydrazine hydrochloride yielded 56% beige crystals from ethanol/toluene, mp > 330 °C; ¹H NMR: 3.54 (s, 2H), 7.05 (d, 8.6 Hz, 1H), 7.29 (dd, 2.0/8.6 Hz, 1H), 7.40 (d, 8.6 Hz, 1H), 7.71 (dd, 2.0/8.6 Hz, 1H), 7.93 (d, 2.0 Hz, 1H), 8.07 (d, 2.0 Hz, 1H), 10.19 (s, 1H), 11.88 (s, 1H); Anal. (C₁₆H₁₀BrIN₂O); C, H, N, Br, I.

3-Methoxy-9-trifluoromethyl-7,12-dihydro-indolo[3,2-*d*][1]benzazepin-6(5*H*)-one (55). Prepared following General Procedure A from 8-methoxy-1*H*-[1]benzazepine-2,5(3*H*,4*H*)-dione³⁵ and 4-trifluorophenylhydrazine. Crystallization from ethanol yielded 25% of a yellow powder, mp > 330 °C; ¹H NMR 3.59 (s, 2H), 3.82 (s, 3H), 6.85 (d, 1H, 2.6 Hz), 6.95 (dd, 1H, 8.9/2.3 Hz), 7.43 (m, 1H), 7.59 (d, 1H, 8.6 Hz), 7.70 (d, 1H, 8.7 Hz), 8.09 (s, 1H), 10.01 (s, 1H), 11.98 (s, 1H); Anal. (C₁₈H₁₃F₃N₂O₂); C, H, N.

5-Hydroxy-8-oxo-8,9-dihydro-7*H*-pyrido[2,3-*b*]azepine-6-carboxylic Acid Ethyl Ester (78). Sodium hydride (640 mg of a 60% suspension in white oil; 16 mmol) was suspended in toluene (5 mL) and heated to 90 °C under nitrogen. A solution of 2-aminopyridine-3-carboxylic acid ethyl ester (76) (664 mg, 4 mmol) and succinic acid diethyl ester (77) (1045 mg, 6 mmol) in toluene (20 mL) was added dropwise, and stirring was continued at 90 °C. The reaction was monitored by TLC (eluent: ethyl acetate). After all the sodium hydride had reacted and completion of the reaction was detected (10 h), the mixture was cooled to room temperature. A 15% solution of acetic acid in water (20 mL) was added dropwise. A precipitate was formed, which was filtered off and washed successively with water and hexanes. Crystallization from ethanol yielded 387 mg (39%) colorless needles, mp 211.5 °C; ¹H NMR 1.31 (t, 3H, 7.1 Hz), 3.03 (s, 2H), 4.31 (q, 2H, 7.1 Hz), 7.34 (dd, 1H, 8.1/4.6 Hz), 8.23 (dd, 1H, 7.9/1.8 Hz), 8.58 (dd, 1H, 4.6/2.0 Hz), 10.72 (bs, 1H), 12.47 (bs, 1H); Anal. (C₁₂H₁₂N₂O₄) C, H, N.

6,7,8,9-Tetrahydro-5*H*-pyrido[2,3-*b*]azepine-5,8-dione (79). A solution of 5-hydroxy-8-oxo-8,9-dihydro-7*H*-pyrido[2,3-*b*]azepine-6-carboxylic acid ethyl ester (78) (372 mg, 1.5 mmol) and water (0.5 mL) in DMSO (15 mL) was stirred at 150 °C under nitrogen. Every 2 h, portions of water (0.5 mL each) were added. After 8 h, the mixture was poured into water (40 mL) and stored at 4 °C overnight. A precipitate was formed, which was filtered off, washed with water, and crystallized from ethanol to yield beige crystals (124 mg, 81%), mp 221 °C; ¹H NMR 2.74–2.77 and 2.93–2.96 (m, AA'XX', 4H), 7.26 (dd, 1H, 7.6/4.6 Hz), 8.26 (dd, 1H, 7.9/1.8 Hz), 8.56 (dd, 1H, 4.6/1.5 Hz), 10.39 (bs, 1H); Anal. (C₉H₈N₂O₂) C, H, N.

9-Chloro-7,12-dihydro-pyrido[2',3':2,3]azepino[4,5-*b*]indol-6(5*H*)-one (61). Prepared following General Procedure A from 6,7,8,9-tetrahydro-5*H*-pyrido[2,3-*b*]azepine-5,8-dione (79) and 4-chlorophenylhydrazine hydrochloride. Crystallization from ethanol yielded 51% of orange crystals, mp > 330 °C; ¹H NMR 3.64 (s, 2H), 7.19 (dd, 1H, 8.6/1.5 Hz), 7.35 (dd, 1H, 7.9/4.8 Hz), 7.46 (d, 1H, 8.6 Hz), 7.82 (d, 1H, 1.5 Hz), 8.16

(dd, 1H, 7.9/1.3 Hz), 8.45 (dd, 1H, 4.6/1.0 Hz), 10.38 (s, 1H), 11.91 (s, 1H); Anal. (C₁₅H₁₀ClN₃O); H, N, C: calcd 63.50; found 63.08.

9-Trifluoromethyl-7,12-dihydro-pyrido[2',3':2,3]azepino[4,5-*b*]indol-6(5*H*)-one (62). Preparation following General Procedure A from 6,7,8,9-tetrahydro-5*H*-pyrido[2,3-*b*]azepine-5,8-dione (79) and 4-trifluoromethylphenylhydrazine yielded 3% of a beige powder after crystallization from ethanol; mp > 330 °C (dec starting at 304 °C); ¹H NMR 3.73 (s, 2H), 7.37 (dd, 1H, 7.6/4.6 Hz), 7.49 (d, 1H, 8.1 Hz), 7.63 (d, 1H, 8.2 Hz), 8.19–8.21 (m, 2H), 8.47 (dd, 1H, 6.8/1.8 Hz), 10.42 (s, 1H), 12.19 (s, 1H); Anal. (C₁₆H₁₀F₃N₃O) (317.27); C, H, N. Preparation of the compound according to General Procedure B yielded 39% of a sample with identical spectral properties.

9-Methyl-7,12-dihydro-pyrido[2',3':2,3]azepino[4,5-*b*]indol-6(5*H*)-one (66). Preparation following General Procedure A from 6,7,8,9-tetrahydro-5*H*-pyrido[2,3-*b*]azepine-5,8-dione (79) and 4-methylphenylhydrazine hydrochloride yielded 64% light yellow needles from ethanol; mp > 330 °C (dec starting at 322 °C); ¹H NMR 2.41 (s, 3H), 3.58 (s, 2H), 7.03 (dd, 1H, 8.1/1.0 Hz), 7.31–7.35 (m, 2H), 7.47 (s, 1H), 8.14 (dd, 1H, 7.6/1.5 Hz), 8.41 (dd, 1H, 4.6/1.5 Hz), 10.30 (s, 1H), 11.55 (s, 1H); Anal. (C₁₆H₁₃N₃O); C, H, N.

9-Methoxy-7,12-dihydro-pyrido[2',3':2,3]azepino[4,5-*b*]indol-6(5*H*)-one (59). A mixture of 6,7,8,9-tetrahydro-5*H*-pyrido[2,3-*b*]azepine-5,8-dione (79) (140 mg; 0.8 mmol), 4-methoxyphenylhydrazine hydrochloride (210 mg, 1.2 mmol), sodium acetate (98 mg; 1.2 mmol), and glacial acetic acid (2 mL) was stirred 2 h at 70 °C. The mixture was poured into 5% aqueous sodium acetate solution (20 mL). The precipitate was filtered off, washed with water, and crystallized from ethanol/toluene to yield 175 mg (78%) orange crystals, mp > 330 °C, (dec starting at 295 °C); ¹H NMR 3.62 (s, 2H), 3.81 (s, 3H), 6.83 (dd, 1H, 8.9/2.3 Hz), 7.21 (d, 1H, 2.6 Hz), 7.31–7.35 (m, 2H), 8.14 (dd, 1H, 7.6/1.5 Hz), 8.41 (dd, 1H, 4.6/1.5 Hz), 10.33 (s, 1H), 11.55 (s, 1H); Anal. (C₁₆H₁₃N₃O₂) C, H, N.

8-Bromo-6,11-dihydro-thieno[3',2':2,3]azepino[4,5-*b*]indol-5(4*H*)-one (71). Preparation according to General Procedure A from 4*H*-thieno[3,2-*b*]azepine-5,8(6*H*,7*H*)-dione⁵⁶ and 4-bromophenylhydrazine hydrochloride yielded 26% of a gray powder after crystallization from ethanol/toluene, mp > 330 °C (dec starting at 293 °C); ¹H NMR 3.54 (s, 2H), 6.94 (d, 1H, 5.6 Hz), 7.24 (dd, 1H, 8.6/2.0 Hz), 7.34 (d, 1H, 8.6 Hz), 7.62 (d, 1H, 5.1 Hz), 7.86 (d, 1H, 1.5 Hz), 10.37 (s, 1H), 11.73 (s, 1H); Anal. (C₁₄H₉BrN₂OS); C, H, N, Br, S.

8-Methyl-6,11-dihydro-thieno[3',2':2,3]azepino[4,5-*b*]indol-5(4*H*)-one (72). Preparation according to General Procedure A from 4*H*-thieno[3,2-*b*]azepine-5,8(6*H*,7*H*)-dione⁵⁶ and 4-methyl-phenylhydrazine hydrochloride yielded 31% brown crystals from ethanol, mp > 330 °C (dec starting at 260 °C); ¹H NMR 2.40 (s, 3H, CH₃), 3.48 (s, 2H), 6.92 (d, 1H, 5.6 Hz), 6.96 (dd, 1H, 8.4/1.3 Hz), 7.26 (d, 1H, 8.1 Hz), 7.39 (s, 1H), 7.57 (d, 1H, 5.6 Hz), 10.31 (s, 1H), 11.37 (s, 1H); Anal. (C₁₅H₁₂N₂OS); C, H, N, S.

8-Chloro-6,11-dihydro-thieno[3',2':2,3]azepino[4,5-*b*]indol-5(4*H*)-one (73). Preparation according to General Procedure A from 4*H*-thieno[3,2-*b*]azepine-5,8(6*H*,7*H*)-dione⁵⁶ and 4-chlorophenylhydrazine hydrochloride yielded 32% of a gray powder from ethanol, mp > 330 °C (dec starting at 295 °C); ¹H NMR 3.71 (s, 2H), 6.94 (d, 1H, 5.1 Hz), 7.13 (dd, 1H, 8.6/2.0 Hz), 7.38 (d, 1H, 8.6 Hz), 7.62 (d, 1H, 5.1 Hz), 7.73 (d, 1H, 2.0 Hz), 10.39 (s, 1H), 11.73 (s, 1H); Anal. (C₁₄H₉ClN₂OS); C, H, N.

General Procedure B for Preparation of Paullones 64, 65, 67, 75 by Thermal-Induced Fischer Indole Reaction from Arylhydrazones. A mixture of an appropriate cyclic ketone (2 mmol), an appropriate arylhydrazine (3 mmol) [or the appropriate substituted arylhydrazine hydrochloride (3 mmol) and sodium acetate (246 mg, 3 mmol)], and glacial acetic acid (20 mL) is stirred for 1 h at 70 °C. After being cooled to room temperature, the mixture is poured into a 5% aqueous sodium acetate solution (40 mL). An arylhydrazone precipitates, which is filtered off and purified by crystallization from ethanol. The arylhydrazone (1 mmol) is then refluxed in the

given amount of diphenyl ether under nitrogen. The reaction is monitored by TLC (eluent: ethyl acetate or toluene/acetone 1:1, respectively). After completion of the reaction, which takes 2–13 h, the solution is cooled to room temperature. Hexane is added until a solid precipitates. The precipitate is filtered off and purified by crystallization from the given solvent.

8-Nitro-6,11-dihydro-thieno[3',2':2,3]azepino[4,5-*b*]indol-5(4*H*)-one (75). According to General Procedure B, 4*H*-thieno[3,2-*b*]azepine-5,8(6*H*,7*H*)-dione⁵⁶ and 4-nitrophenylhydrazine hydrochloride were reacted to give an arylhydrazone (51%; mp 277 °C (dec)), which was converted in refluxing diphenyl ether (150 mL, 3 h) to yield 189 mg (63%) of a brown powder after crystallization from ethanol, mp > 330 °C; ¹H NMR 3.67 (s, 2H), 6.97 (d, 1H, 5.1 Hz), 7.54 (d, 1H, 8.7 Hz), 7.70 (d, 1H, 5.1 Hz), 8.04 (dd, 1H, 8.9/2.3 Hz), 8.68 (d, 1H, 2.0 Hz), 10.50 (s, 1H), 12.34 (s, 1H); EI/HRMS (C₁₄H₉N₃O₃S) calcd 299.0365, found 299.0363.

3-Methoxy-9-nitro-7,12-dihydro-indolo[3,2-*d*][1]benzazepin-6(5*H*)-one (64). According to General Procedure B, 8-methoxy-1*H*-(1)benzazepine-2,5(3*H*,4*H*)-dione³⁵ and 4-nitrophenylhydrazine hydrochloride were reacted to give an arylhydrazone (64%, mp 283–284 °C (dec)), which was converted in refluxing diphenyl ether (40 mL, 2h) to yield the title compound. Purification by column chromatography (ethyl acetate) and subsequent crystallization from ethanol/toluene yielded 13% dark brown crystals, mp > 330 °C; ¹H NMR 3.63 (s, 2H), 3.82 (s, 3H), 6.86 (d, 1H, 2.0 Hz), 6.96 (dd, 1H, 8.9/2.3 Hz), 7.56 (d, 1H, 9.1), 7.70 (d, 1H, 8.6 Hz), 8.04 (dd, 1H, 9.2/2.0), 8.69 (d, 1H, 2.0 Hz), 10.13 (s, 1H), 12.29 (s, 1H); C₁₇H₁₃N₃O₄ (323.31); HRFAB-MS: calcd 323.0906; found 323.0909.

2-Methoxy-9-nitro-7,12-dihydro-indolo[3,2-*d*][1]benzazepin-6(5*H*)-one (65). According to General Procedure B, 7-methoxy-1*H*-(1)benzazepine-2,5(3*H*,4*H*)-dione³⁵ and 4-nitrophenylhydrazine hydrochloride were reacted to give an arylhydrazone (60%, mp 274 °C (dec)), which was converted in refluxing diphenyl ether (40 mL, 2h) to yield the title compound. Purification by column chromatography (ethyl acetate) and subsequent crystallization from ethanol/toluene yielded 23% dark brown crystals, mp > 330 °C; ¹H NMR 3.61 (s, 2H), 3.86 (s, 3H), 7.06 (dd, 1H, 8.9/2.8 Hz), 7.22 (d, 1H, 8.6 Hz), 7.32 (d, 1H, 2.6 Hz), 7.61 (d, 1H, 8.6 Hz), 8.08 (dd, 1H, 9.2/2.0 Hz), 8.76 (d, 1H, 1.5 Hz), 10.03 (s, 1H), 12.41 (s, 1H); Anal. (C₁₇H₁₃N₃O₄); H, N; C calcd. 63.16, found 62.55.

7,12-Dihydro-pyrido[3',2':4,5]pyrrolo[3,2-*d*][1]benzazepin-6(5*H*)-one (67). 1*H*-(1)Benzazepine-2,5(3*H*,4*H*)-dione (175 mg, 1 mmol)⁵⁶ and 2-hydrazinopyridine (164 mg, 1.5 mmol) were stirred in 10 mL glacial acetic acid at 70 °C for 7 h. Water (50 mL) was added and the mixture was neutralized with concentrated ammonium hydroxide solution. An arylhydrazone precipitated, which was filtered off and purified by crystallization from ethanol to yield 51% colorless crystals, mp 233 °C. This material was converted following General Procedure B in refluxing diphenyl ether (20 mL, 2 h) to yield the title compound. Crystallization from ethanol/toluene yielded 58% colorless crystals, mp > 330 °C; ¹H NMR 3.52 (s, 2H), 7.13 (dd, 8.1/4.6 Hz, 1H), 7.27 ("t", 8.4 Hz, 2H), 7.38–7.42 (m, 1H), 7.80 (d, 7.6 Hz, 1H), 8.12 (d, 7.6 Hz, 1H), 8.27 (dd, 4.6/1.0 Hz, 1H), 10.16 (s, 1H), 12.20 (s, 1H); Anal. (C₁₅H₁₁N₃O) C, H, N.

9-Nitro-7,12-dihydro-indolo[3,2-*d*][1]benzazepine-6(5*H*)-thione (68). To a stirred solution of 9-nitro-7,12-dihydro-indolo[3,2-*d*][1]benzazepin-6(5*H*)-one (alsterpaullone (1); 293 mg, 1 mmol) in dry THF (30 mL) were added successively P₂S₅ (250 mg; 1.12 mmol) and NaHCO₃ (370 mg; 4.4 mmol) at 50 °C under nitrogen. The mixture was refluxed for 3 h, cooled to room temperature, and poured on crushed ice (50 mL). The precipitate was filtered off, washed with water, and crystallized from ethanol to yield 136 mg (44%) of a yellow powder, mp > 330 °C (dec starting at 285 °C); ¹H NMR 4.04 (s, 2H), 7.43–7.52 (m, 3H), 7.63 (d, 1H, 8.6 Hz), 7.83 (d, 1H, 7.1 Hz), 8.10 (dd, 1H, 9.1/2.0 Hz), 8.68 (d, 1H, 2.5 Hz), 12.17 (s, 1H), 12.51 (s, 1H); Anal. (C₁₆H₁₁N₃O₂S) C, H, N.

12-Methyl-6-methylthio-9-nitro-7,12-dihydro-indolo[3,2-*d*][1]benzazepine (69). A suspension of 9-nitro-7,12-

dihydro-indolo[3,2-*d*][1]benzazepine-6(5*H*)-thione (68) (108 mg, 0.35 mmol) and sodium hydride (15 mg of a 60% suspension in white oil) in dry THF (10 mL) was stirred for 15 min under nitrogen. After addition of iodomethane (60 mg, 0.42 mmol), the mixture was refluxed under nitrogen. After 1, 1.5, and 3 h, the addition of iodomethane (60 mg, 0.42 mmol) was repeated. Furthermore, sodium hydride (15 mg of a 60% suspension in white oil) was added after 2 h of refluxing. The reaction was monitored by TLC (eluent: ethyl acetate). After completion of the reaction 4 h, the mixture was poured into ice water (50 mL). The precipitate was filtered off and crystallized from ethanol to yield 55 mg (47%) light brown crystals, mp 237 °C; ¹H NMR 2.33 (s, 3H), 2.84 (bs, 1H), 3.95 (s, 3H), 4.31 (bs, 1H), 7.33 ("dt", 1H, 7.6/1.3 Hz), 7.41 (d, 1H, 8.1 Hz), 7.49 ("dt", 1H, 7.6/1.0 Hz), 7.77 (d, 1H, 9.2 Hz), 7.83 (d, 1H, 7.6 Hz), 8.13 (dd, 1H, 9.2/2.5 Hz), 8.88 (d, 1H, 2.0 Hz); Anal. (C₁₈H₁₅N₃O₂S) C, H, N.

2-(2-Propenyl)-9-trifluoromethyl-7,12-dihydroindolo[3,2-*d*][1]benzazepin-6(5*H*)-one (80). To a mixture of 2-iodo-9-trifluoromethyl-7,12-dihydro-indolo[3,2-*d*][1]benzazepin-6(5*H*)-one (38)²³ (482 mg, 1.09 mmol), PdCl₂(PPh₃)₂ (70 mg, 0.1 mmol), PPh₃ (52 mg, 0.2 mmol) and 2,4-di-*tert*-butyl-4-methylphenol (6 crystals) in DMF (10 mL) was added allyltributyltin (410 mg, 1.24 mmol) under nitrogen. The corresponding mixture was stirred at room temperature for 5 min and then heated to 95 °C for 1.5 h. After being cooled to room temperature, the mixture was poured into ice water. A solid precipitated, which was filtered off with suction, washed with cyclohexane and water, and purified by column chromatography to give 132 mg of 2-tributylstannyl-9-trifluoromethyl-7,12-dihydroindolo[3,2-*d*][1]benzazepin-6(5*H*)-one (20%) as a side product and 273 mg (70%) of the title compound, mp > 330 °C; ¹H NMR 3.45 (d, 6.6 Hz, 2H), 3.59 (s, 2H), 5.11 (dd, 10.0/1.0 Hz, 1H), 5.16 (dd, 16.8/1.6 Hz, 1H), 5.99–6.09 (m, 1H), 7.20–7.26 (m, 2H), 7.45 (dd, 8.6 Hz/1.0 Hz, 1H), 7.59–7.62 (m, 2H), 8.13 (s, 1H), 10.10 (s, 1H), 12.06 (s, 1H); Anal. (C₂₀H₁₅N₂O₂F₃) C, H, N.

2-(2-Oxopropyl)-9-trifluoromethyl-7,12-dihydroindolo[3,2-*d*][1]benzazepin-6(5*H*)-one (60). To a solution of 2-(2-propenyl)-9-trifluoromethyl-7,12-dihydroindolo[3,2-*d*][1]benzazepin-6(5*H*)-one (80) (108 mg, 0.3 mmol) in DMF (6 mL) and H₂O (1 mL) was added PdCl₂ (6 mg, 0.03 mmol) and CuCl₂ (48 mg, 0.36 mmol). After the mixture was stirred overnight at room temperature, it was poured into 30 mL of water and extracted with ethyl acetate (50 mL × 3). The organic layers were combined, washed with water (10 mL × 3), and dried over Na₂SO₄. Evaporation of the solution yielded a residue, which was purified by flash chromatography (ethyl acetate: petroleum ether = 70:30) to yield 78 mg (69%) of the title compound, mp 295–297 °C (ethanol); ¹H NMR 2.20 (s, 3H), 3.58 (s, 2H), 3.78 (s, 2H), 7.18–7.30 (m, 2H), 7.46 (d, 8.6 Hz, 1H), 7.57 (s, 1H), 7.61 (d, 8.1 Hz, 1H), 8.13 (s, 1H), 10.14 (s, 1H), 12.07 (s, 1H); Anal. (C₂₀H₁₅N₂O₂F₃) C, H, N.

General Procedure C for the Synthesis of Cyano Derivatives 54, 63, 74, from Corresponding Bromo Compounds. A mixture of the bromo-substituted paullone derivative (1 mmol) and copper(I) cyanide (180 mg, 2 mmol) in *N*-methyl-2-pyrrolidone (10 mL) is refluxed for 2 h. After the mixture is cooled to room temperature, water (10 mL) is added. The precipitate is filtered off with suction and washed with water. The precipitate is then suspended in a mixture of water (10 mL) and 1,2-diaminoethane (2.5 mL). After stirring for 15 min, the solid is filtered off with suction, washed twice with 10% aqueous sodium cyanide solution, and purified by crystallization from the given solvent.

3-Methoxy-6-oxo-5,6,7,12-tetrahydro-indolo[3,2-*d*][1]benzazepine-9-carbonitrile (63). Preparation following General Procedure C from 9-bromo-3-methoxy-7,12-dihydro-indolo[3,2-*d*][1]benzazepin-6(5*H*)-one³⁵ yielded 25% brown crystals after purification by column chromatography (ethyl acetate) and crystallization from ethanol/toluene; mp > 330 °C; ¹H NMR 3.57 (s, 2H), 3.82 (s, 3H), 6.85 (d, 1H, 2.52 Hz), 6.94 (dd, 1H, 8.64/2.56 Hz), 7.48 (dd, 1H, 8.36/1.26 Hz), 7.56 (d, 1H, 8.64

Hz), 7.69 (d, 1H, 8.64 Hz), 8.27 (s, 1H), 10.10 (s, 1H), 12.13 (s, 1H); HRFAB-MS ($C_{18}H_{13}N_3O_2$) calcd 303.1008; found 303.1012.

5-Oxo-4,5,6,11-tetrahydro-thieno[3',2':2,3]azepino[4,5-*b*]indole-8-carbonitrile (74). Preparation following General Procedure C from 8-bromo-6,11-dihydro-thieno[3',2':2,3]azepino[4,5-*b*]indol-5(4*H*)-one (**53**) yielded 23% of a beige powder after crystallization from ethanol, mp > 330 °C; 1H NMR 3.60 (s, 2H), 6.96 (d, 1H, 5.1 Hz), 7.48 (dd, 1H, 8.6/1.6 Hz), 7.55 (d, 1H, 8.1 Hz), 7.67 (d, 1H, 5.1 Hz), 8.27 (s, 1H), 10.46 (s, 1H), 12.15 (s, 1H); EI/HRMS ($C_{15}H_9N_3OS$) calcd 279.0466; found 279.0458.

6-Oxo-5,6,7,12-tetrahydro-indolo[3,2-*d*][1]benzazepine-2-carbonitrile (54). Preparation following General Procedure C from 2-bromo-7,12-dihydro-indolo[3,2-*d*][1]benzazepin-6(5*H*)-one²² yielded 47% beige crystals after crystallization from ethanol/toluene, mp > 330 °C; 1H NMR 3.62 (s, 2H), 7.09–7.12 (m, 1H) 7.19–7.24 (m, 1H), 7.39 (d, 8.1 Hz, 1H), 7.46 (d, 7.6 Hz, 1H), 7.71 (d, 7.6 Hz, 1H), 7.81 (dd, 8.4/1.8 Hz, 1H), 8.2 (d, 2.0 Hz, 1H), 10.56 (s, 1H), 11.72 (s, 1H); Anal. ($C_{17}H_{11}N_3O$) C, H, N: calcd 15.38, found 14.84.

9-Amino-7,12-dihydro-indolo[3,2-*d*][1]benzazepin-6(5*H*)-one (65). To a suspension of 9-nitro-7,12-dihydro-indolo[3,2-*d*][1]benzazepin-6(5*H*)-one (alsterpaullone (**1**); 293 mg, 1 mmol) in ethanol (10 mL) a suspension of $CaCl_2$ (70 mg) and zinc powder (2.1 g) in water (1.8 mL) was added. After being refluxed for 1 h, the mixture was filtered. The filter cake was extracted with ethyl acetate (10 mL). The combined organic layers were dried by means of sodium sulfate and evaporated to dryness. The residue was crystallized from ethanol to yield 35% brown crystals, mp 254 °C (dec); 1H NMR 3.33 (br. s, 2H), 4.58 (s, 2H) 6.57 (dd, 1H, 8.4/1.8 Hz), 6.72 (m, 1H), 7.13 (d, 1H, 8.6 Hz), 7.20–7.34 (m, 3H), 7.68 (d, 1H, 7.6 Hz), 10.01 (s, 1H), 11.06 (s, 1H); Anal. ($C_{16}H_{13}N_3O \cdot 1H_2O$); C, H, N: calcd 14.94; found 13.31.

9-Acetamido-7,12-dihydro-indolo[3,2-*d*][1]benzazepin-6(5*H*)-one (58). To a refluxing solution of 9-nitro-7,12-dihydro-indolo[3,2-*d*][1]benzazepin-6(5*H*)-one (alsterpaullone (**1**); 220 mg, 0.75 mmol) and water (0.35 mL) in glacial acetic acid (10 mL) was added iron powder (229 mg) portionwise over 75 min. After 45 min, another portion of water (0.35 mL) was added. After being refluxed for overall 6 h, the mixture was cooled to room temperature and diluted with water (10 mL) and extracted with ethyl acetate (3 \times 10 mL). The combined organic layers were washed with water and aqueous 10% Na_2CO_3 solution, dried (Na_2SO_4), and evaporated. The residue was crystallized from ethanol to yield 37% of a gray powder, mp > 330 °C; 1H NMR 2.05 (s, 3H), 3.41 (s, 2H), 7.24–7.38 (m, 5H), 7.72 (d, 1H, 7.1 Hz), 7.94 (s, 1H), 9.81 (s, 1H), 10.10 (s, 1H), 11.50 (s, 1H); Anal. ($C_{18}H_{15}N_3O_2$) H, N, C: calcd 70.81; found 70.30.

Kinase Assays. Reagents. Homogenization buffer: 60 mM β -glycerophosphate, 15 mM *p*-nitrophenyl phosphate, 25 mM Mops (pH 7.2), 15 mM EGTA, 15 mM $MgCl_2$, 1 mM dithiothreitol, 1 mM sodium vanadate, 1 mM NaF, 1 mM phenyl phosphate, 10 μ g leupeptin mL^{-1} , 10 μ g aprotinin mL^{-1} , 10 μ g soybean trypsin inhibitor mL^{-1} , and 100 μ g benzamidine. Buffer A: 10 mM $MgCl_2$, 1 mM EGTA, 1 mM dithiothreitol, 25 mM Tris/HCl pH 7.5, 50 μ g heparin mL^{-1} . Buffer C: homogenization buffer but 5 mM EGTA, no NaF and no protease inhibitors.

Kinase activities were assayed in duplicates in buffer A or C at 30 °C, at a final ATP concentration of 15 μ M. The order of mixing the reagents was buffers, substrate, enzyme, and inhibitor. There was no preincubation at 30 °C. Addition of ATP was considered as time 0 of the incubation period. Assays were run under conditions where less than 5% of the radio-labeled phosphate was incorporated. Blank values were subtracted and activities calculated as pmol of phosphate incorporated for a 10-min incubation. The activities are usually expressed in percentage of the maximal activity, i.e., in the absence of inhibitors. Controls were performed with appropriate dilutions of DMSO.

GSK-3 β . GSK-3 β was expressed in and purified from insect sf9 cells.⁵⁷ It was assayed, following a 1/100 dilution in 1 mg

BSA per mL 10 mM dithiothreitol, with 5 μ L 40 μ M GS-1 peptide as a substrate, in buffer A, in the presence of 15 μ M [γ - ^{32}P]ATP (3000 Ci \cdot mmol $^{-1}$; 1 mCi \cdot mL $^{-1}$) in a final volume of 30 μ L. The GS-1 peptide (YRRRAVPPSPSLSRHSSPHQS-pEEDDEE) was synthesized by the Peptide Synthesis Unit, Institute of Biomolecular Sciences, University of Southampton, Southampton SO16 7PX, U.K. After 30 min incubation at 30 °C, 25 μ L aliquots of supernatant were spotted onto 2.5 \times 3 cm pieces of Whatman P81 phosphocellulose paper, and, 20 s later, the filters were washed five times (for at least 5 min each time) in a solution of 10 mL of phosphoric acid per liter of water. The wet filters were counted in the presence of 1 mL of ACS (Amersham) scintillation fluid.

CDK1/Cyclin B. CDK1/cyclin B was extracted in homogenization buffer from M phase starfish (*Marthasterias glacialis*) oocytes and purified by affinity chromatography on $p9^{CKShs1}$ -Sephacrose beads, from which it was eluted by free $p9^{CKShs1}$ as previously described.^{58,59} The kinase activity was assayed in buffer C, with 1 mg histone H1 (Type III-S, Sigma Chemicals) per mL, in the presence of 15 μ M [γ - ^{32}P]ATP (3000 Ci \cdot mmol $^{-1}$; 1 mCi \cdot mL $^{-1}$) in a final volume of 30 μ L. After a 10-min incubation at 30 °C, 25 μ L aliquots of supernatant were spotted onto P81 phosphocellulose papers and treated as described above.

CDK5/p25. CDK5/p25 was reconstituted by mixing equal amounts of recombinant mammalian CDK5 and p25 expressed in *E. coli* as GST (glutathione S-transferase) fusion proteins and purified by affinity chromatography on glutathione-agarose (vectors kindly provided by J. H. Wang, Department of Medical Chemistry, University of Calgary, Alberta, Canada) (p25 is a truncated version of the p35, the 35-kDa CDK5 activator). Its activity was assayed in buffer C as described for CDK1/cyclin B.

Acknowledgment. X.X. and C.K. gratefully acknowledge financial funding by the National Cancer Institute. This research was also supported by a grant from the "Association pour la Recherche sur le Cancer" (ARC 5343) (L.M.) and a grant ("Molécules & Cibles Thérapeutiques") from the "Ministère de la Recherche/INSERM/CNRS" (L.M.).

References

- Ali, A.; Hoefflich, K. P.; Woodgett, J. R. Glycogen synthase kinase-3: properties, function and regulation. *Chem. Rev.* **2001**, *101*, 2527–2540.
- Doble, B. W.; Woodgett, J. R. GSK-3: tricks of the trade for a multi-tasking kinase. *J. Cell Sci.* **2003**, *116*, 1175–1186.
- Frame, S.; Cohen, P. GSK3 takes center stage more than 20 years after its discovery. *Biochem. J.* **2001**, *359*, 1–16.
- Martinez, A.; Castro, A.; Dorronsoro, I.; Alonso, M. Glycogen synthase kinase 3 (GSK-3) inhibitors as new promising drugs for diabetes, neurodegeneration, cancer, and inflammation. *Med. Res. Rev.* **2002**, *22*, 373–384.
- Cohen, P. The Croonian Lecture 1998. Identification of a protein cascade of major importance in insulin signal transduction. *Philos. Trans. R. Soc. London B* **1999**, *354*, 485–495.
- Wagmann, A. S.; Nuss, J. M. Current therapies and emerging targets for the treatment of diabetes. *Curr. Pharm. Des.* **2001**, *7*, 417–450.
- Ryves, W. J.; Harwood, A. J. Lithium inhibits glycogen synthase kinase-3 by competition for magnesium. *Biochem. Biophys. Res. Commun.* **2001**, *280*, 720–725.
- Nikoulina, S. E.; Ciaraldi, T. P.; Mudaliar, S.; Carter, L.; Johnson, K.; Henry, R. R. Inhibition of glycogen synthase kinase 3 improves insulin action and glucose metabolism in human skeletal muscle. *Diabetes* **2002**, *51*, 2190–2198.
- Naerum, L.; Nørskov-Lauritsen, L.; Olesen, P. H. Scaffold hopping and optimization towards libraries of glycogen synthase kinase-3 inhibitors. *Bioorg. Med. Chem. Lett.* **2002**, *12*, 1525–1528.
- Martinez, A.; Alonso, M.; Castro, A.; Perez, C.; Moreno, F. First non-ATP competitive glycogen synthase kinase-3b (GSK-3b) inhibitors: thiazolidinones (TDZD) as potential drugs for the treatment of Alzheimer's disease. *J. Med. Chem.* **2002**, *45*, 1292–1299.
- Smith, D. G.; Ward, R. W. Preparation of diamino-1,2,4-triazole-carboxylic acid and derivatives as GSK-3 inhibitors. *PCT Int. Appl.* WO 0109106, 2001.

- (12) Coghlan, M. P.; Culbert, A. A.; Cross, D. A. E.; Corcoran, S. L.; Yates, J. D.; Pearce, N. J.; Rausch, O. L.; Murphy, G. J.; Carter, P. S.; Cox, L. R.; Mills, D.; Brown, M. J.; Haigh, D.; Ward, R. W.; Smith, D. G.; Murray, K. J.; Reith, A. D.; Holder, J. Selective small molecule inhibitors of glycogen synthase kinase-3 modulate glycogen metabolism and gene transcription. *Chem. Biol.* **2000**, *7*, 793–803.
- (13) Smith, D. G.; Buffet, M.; Fenwick, A. E.; Haigh, D.; Ife, R. J.; Saunders, M.; Slingsby, B. P.; Stacey, R.; Ward, R. W. 3-Anilino-4-arymaleimides: potent and selective inhibitors of glycogen synthase kinase-3 (GSK-3). *Bioorg. Med. Chem. Lett.* **2001**, *11*, 635–639.
- (14) Meijer, L.; Thunissen, A.-M. W. H.; White, A. W.; Garnier, M.; Nikolic, M.; Tsai, L.-H.; Walter, J.; Cleverley, K. E.; Salinas, P. C.; Wu, Y.-Z.; Biernat, J.; Mandelkow, E. M.; Kim, S.-H.; Pettit, G. R. Inhibition of cyclin-dependent kinases, GSK-3 β and CK1 by hymenialdisine, a marine sponge constituent. *Chem. Biol.* **2000**, *7*, 51–63.
- (15) Hoessel, R.; Leclerc, S.; Endicott, J.; Nobel, M. E. M.; Lawrie, A.; Tunnah, P.; Leost, M.; Damiens, E.; Marie, D.; Marko, D.; Niederberger, E.; Tang, W.; Eisenbrand, G.; Meijer, L. Indirubin, the active constituent of a Chinese antileukaemia medicine, inhibits cyclin-dependent kinases. *Nature Cell Biol.* **1999**, *1*, 60–67.
- (16) Leclerc, S.; Garnier, M.; Hoessel, R.; Marko, D.; Bibb, J. A.; Snyder, G. L.; Greengard, P.; Biernat, J.; Wu, Y.-Z.; Mandelkow, E.-M.; Eisenbrand, G.; Meijer, L. Indirubins inhibit glycogen kinase-3 β and CDK5/p25, two protein kinases involved in abnormal tau phosphorylation in Alzheimer's disease. *J. Biol. Chem.* **2001**, *276*, 251–260.
- (17) Damiens, E.; Baratte, B.; Marie, D.; Eisenbrand, G.; Meijer, L. Anti-mitotic properties of indirubin-3'-monoxime, a CDK/GSK-3 inhibitor: induction of endoreplication following prophase arrest. *Oncogene* **2001**, *20*, 3786–3797.
- (18) Marko, D.; Schätzle, S.; Friedel, A.; Genzlinger, A.; Zankl, H.; Meijer, L.; Eisenbrand, G. Inhibition of cyclin-dependent kinase 1 (CDK1) by indirubin derivatives in human tumour cells. *Br. J. Cancer* **2001**, *84*, 283–289.
- (19) Mettrey, Y.; Gompel, M.; Thomas, V.; Garnier, M.; Leost, M.; Ceballos-Picot, I.; Noble, M.; Endicott, J.; Vierfond, J.-M.; Meijer, L. Aloisines, a new family of CDK/GSK-3 inhibitors. SAR study, crystal structure in complex with CDK2, enzyme selectivity, and cellular effects. *J. Med. Chem.* **2003**, *46*, 222–236.
- (20) Leost, M.; Schultz, C.; Link, A.; Wu, Y.-Z.; Biernat, J.; Mandelkow, E.-M.; Bibb, J. A.; Snyder, G. L.; Greengard, P.; Zaharevitz, D. W.; Gussio, R.; Senderowicz, A. M.; Sausville, E. A.; Kunick, C.; Meijer, L. Paullones are potent inhibitors of glycogen synthase kinase-3 β and cyclin-dependent kinase 5/p25. *Eur. J. Biochem.* **2000**, *267*, 5983–5994.
- (21) Zaharevitz, D. W.; Gussio, R.; Leost, M.; Senderowicz, A. M.; Lahusen, T.; Kunick, C.; Meijer, L.; Sausville, E. A. Discovery and initial characterization of the paullones, a novel class of small-molecule inhibitors of cyclin-dependent kinases. *Cancer Res.* **1999**, *59*, 2566–2569.
- (22) Schultz, C.; Link, A.; Leost, M.; Zaharevitz, D. W.; Gussio, R.; Sausville, E. A.; Meijer, L.; Kunick, C. Paullones, a series of cyclin-dependent kinase inhibitors: Synthesis, evaluation of CDK1/Cyclin B inhibition, and in vitro antitumor activity. *J. Med. Chem.* **1999**, *42*, 2909–2919.
- (23) Kunick, C.; Schultz, C.; Lemcke, T.; Zaharevitz, D. W.; Gussio, R.; Jalluri, R. K.; Sausville, E. A.; Leost, M.; Meijer, L. 2-Substituted paullones: CDK1/cyclin B-inhibiting property and in vivo antiproliferative activity. *Bioorg. Med. Chem. Lett.* **2000**, *10*, 567–569.
- (24) Gussio, R.; Zaharevitz, D. W.; McGrath, C. F.; Pattabiraman, N.; Kellogg, G. E.; Schultz, C.; Link, A.; Kunick, C.; Leost, M.; Meijer, L.; Sausville, E. A. Structure-based design modifications of the paullone molecular scaffold for cyclin-dependent kinase inhibition. *Anti-Cancer Drug Des.* **2000**, *15*, 53–66. Kenpaullone was manually docked into the CDK1/cyclin B model and the protein–ligand complex was iteratively minimized using several cycles of minimization with the CFF91 force field and refining with hydrophobic analysis (HINT).
- (25) Mandelkow, E. M.; Mandelkow, E. Tau in Alzheimer's disease. *Trends Cell Biol.* **1998**, *8*, 425–427.
- (26) Patrick, G. N.; Zukerberg, L.; Nikolic, M.; de la Monte, S.; Dikkes, P.; Tsai, L.-H. Conversion of p35 to p25 deregulates Cdk5 activity and promotes neurodegeneration. *Nature* **1999**, *402*, 615–622.
- (27) Mandelkow, E. The tangled tale of tau. *Science* **1999**, *402*, 588–589.
- (28) Coleman, K. G.; Lyssikatos, J. P.; Ynag, B. V. Chemical inhibitors of cyclin-dependent kinases. *Annual Reports in Medicinal Chemistry*; Bristol, J. A., Ed.; Academic Press: San Diego, 1997; Vol. 32, pp 171–179.
- (29) Meijer, L. Cyclin-dependent kinase inhibitors as potential anticancer, antineurodegenerative, antiviral and antiparasitic agents. *Drug Resist. Update* **2000**, *3*, 83–88.
- (30) Klebe, G.; Abraham, U.; Mietzner, T. Molecular similarity indices in a comparative Analysis (CoMSIA) of drug molecules to correlate and predict their biological activity. *J. Med. Chem.* **1994**, *37*, 4130–4146.
- (31) Böhm, M.; Stürzebecher, J.; Klebe, G. Three-Dimensional Quantitative Structure–Activity Relationship Analyses Using Comparative Molecular Field Analysis and Comparative Molecular Similarity Indices Analysis To Elucidate Selectivity Differences of Inhibitors Binding to Trypsin, Thrombin, and Factor Xa. *J. Med. Chem.* **1999**, *42*, 458–477.
- (32) Klebe, G.; Abraham, U. Comparative molecular similarity index analysis (CoMSIA) to study hydrogen-bonding properties and to score combinatorial libraries. *J. Comput.-Aided Mol. Des.* **1999**, *13*, 1–10.
- (33) Ducrot, P.; Legraverend, M.; Grierson, D. S. 3D-QSAR CoMFA on cyclin-dependent kinase inhibitors. *J. Med. Chem.* **2000**, *43*, 4098–4108.
- (34) Naumann, T.; Matter, H. Structural classification of protein kinases using 3D molecular interaction field analysis of their ligand binding sites: target family landscapes. *J. Med. Chem.* **2002**, *45*, 2366–2378.
- (35) Wieking, K.; Knockaert, M.; Leost, M.; Zaharevitz, D. W.; Meijer, L.; Kunick, C. Synthesis of paullones with aminoalkyl side chains. *Arch. Pharm. Pharm. Med. Chem.* **2002**, *335*, 311–317.
- (36) Kunick, C. Synthese von 7,12-Dihydro-indolo[3,2-d][1]benzazepin-6(5H)-onen und 6,11-Dihydro-thieno[3',2':2,3]azepino[4,5-b]indol-5(4H)-on. *Arch. Pharm. (Weinheim)* **1992**, *325*, 297–299.
- (37) Knockaert, M.; Wieking, K.; Schmitt, S.; Leost, M.; Grant, K. M.; Mottram, J. C.; Kunick, C.; Meijer, L. Intracellular targets of paullones: Identification following affinity purification on immobilized inhibitor. *J. Biol. Chem.* **2002**, *277*, 25493–25501.
- (38) Nguyen, C. H.; Marchand, C.; Delage, S.; Sun, J.-S.; Garestier, T.; Hélène, C.; Bisagni, E. Synthesis of 13H-benzo[6,7]- and 13H-benzo[4,5]indolo[3,2-c]quinolines: a new series of potent specific ligands for triplex DNA. *J. Am. Chem. Soc.* **1998**, *120*, 2501–2507.
- (39) MacPhillamy, H. B.; Dziemian, R. L.; Lucas, R. A.; Kuehne, M. E. The alkaloids of *Tabernanthe iboga*. Part VI. The synthesis of the selenium dehydrogenation products from ibogamine. *J. Am. Chem. Soc.* **1958**, *80*, 2172–2178.
- (40) von Braun, J.; Manz, G. Fluoranthen und seine Derivate. *Liebigs Ann. Chem.* **1931**, *488*, 111–126.
- (41) Newman, M. S.; Boden, H. N-methylpyrrolidone as solvent for reaction of aryl halides with cuprous cyanide. *J. Org. Chem.* **1961**, *26*, 2525.
- (42) SYBYL molecular modeling software; version 6.8; Tripos Associated Ltd.: St. Louis, MO.
- (43) Stewart, J. J. MOPAC: a semiempirical molecular orbital program. *J. Comput.-Aided Mol. Des.* **1990**, *4*, 1–105.
- (44) Clark, M.; Cramer, R. D., III; Van Oobdenbosch, N. The Tripos Forcefield. *J. Comput. Chem.* **1989**, *10*, 982–1012.
- (45) Gerber, P. R.; Müller, K. MAB, a generally applicable molecular force field for structure modelling in medicinal chemistry. *J. Comput.-Aided Mol. Des.* **1995**, *9*, 251–268.
- (46) Gerber, P. R. Charge distribution from a simple molecular orbital type calculation and non-bonding interaction terms in the force field MAB. *J. Comput.-Aided Mol. Des.* **1998**, *12*, 37–51.
- (47) Wold, S.; Albano, C.; W. J. Dunn, I.; Ellund, U.; Esbensen, K.; Geladi, P.; Hellberg, S.; Johansson, E.; Lindberg, W.; Sjostrom, M. Multivariate Data Analysis in Chemistry. *Chemometrics: Mathematics and Statistics in Chemistry*; Reidel: Dordrecht, Netherlands, 1984.
- (48) Bush, B. L.; Nachbar, R. B., Jr. Sample-distance partial least squares: PLS optimized for many variables, with application to CoMFA. *J. Comput.-Aided Mol. Des.* **1993**, *7*, 587–619.
- (49) Thompson, J. D.; Higgins, D. G.; Gibson, T. J. CLUSTAL W: improving the selectivity of progressive multiple sequence alignment through sequence weighting, position-specific gap penalties and weight matrix choice. *Nucleic Acid Res.* **1994**, *22*, 4673–4680.
- (50) Okumura, E.; Sekiai, T.; Hisanaga, S.; Tachibana, K.; Kishimoto, T. Initial triggering of M-phase in starfish oocytes: a possible novel component of maturation-promoting factor besides cdc2 kinase. *J. Cell. Biol.* **1996**, *132*, 125–135.
- (51) Meyerson, M.; Enders, G. H.; Wu, C. L.; Su, L. K.; Gorka, C.; Nelson, C.; Harlow, E.; Tsai, L. H. A family of human cdc2-related protein kinases. *EMBO J.* **1992**, *11*, 2909–2917.
- (52) Stambolic, V.; Woodgett, J. R. Mitogen inactivation of glycogen synthase kinase-3 β in intact cells via serine 9 phosphorylation. *Biochem. J.* **1994**, *303* (Pt 3), 701–704.
- (53) Boeckmann, B.; Bairoch, A.; Apweiler, R.; Blatter, M. C.; Estreicher, A.; Gasteiger, E.; Martin, M. J.; Michoud, K.; O'Donovan, C.; Phan, I.; Pilbout, S.; Schneider, M. The SWISS-PROT protein knowledgebase and its supplement TrEMBL in 2003. *Nucleic Acid Res.* **2003**, *31*, 365–370.
- (54) Lemcke, T.; Kunick, C.; Joergensen, F. S. 3D-QSAR Analysis of the CDK-inhibiting activity of paullones. *Arch. Pharm. Pharm. Med. Chem.* **2001**, *334*, 41.

- (55) Zhu, L.; Hou, T.; Xu, X. Three-dimensional quantitative structure–activity relationship study on paullones as cdk inhibitors using CoMSIA and CoMFA. *J. Mol. Model.* **2001**, 223–230.
- (56) Kunick, C. Synthese [b]-kondensierter Azepindione durch Dealkoxycarbonylierung. *Arch. Pharm. (Weinheim)* **1991**, 324, 579–581.
- (57) Hughes, K.; Pulverer, B. J.; Theocharous, P.; Woodgett, J. R. Baculovirus-mediated expression and characterisation of rat glycogene synthase kinase-3b, the mammalian homologue of the *Drosophila melanogaster* zestewhite homeotic gene product. *Eur. J. Biochem.* **1992**, 203, 305–311.
- (58) Meijer, L.; Borgne, A.; Mulner, O.; Chong, J. P. J.; Blow, J. J.; Inagaki, N.; Inagaki, M.; Delcros, J.-G.; Moulinoux, J.-P. Biochemical and cellular effects of roscovitine, a potent and selective inhibitor of the cyclin-dependent kinases cdc2, cdk2 and cdk5. *Eur. J. Biochem.* **1997**, 243, 527–536.
- (59) Borgne, A.; Ostvold, A. C.; Flament, S.; Meijer, L. Intra-M phase promoting factor phosphorylation of cyclin B at the prophase/metaphase transition. *J. Biol. Chem.* **1999**, 274, 11977–11986.

JM0308904